SCIENCE CHINA
Information Sciences

• REVIEW •

February 2021, Vol. 64 121301:1–121301:24
https://doi.org/10.1007/s11432-020-3084-1

Multimodal hyperspectral remote sensing: an overview and perspective

Yanfeng GU[1,2], Tianzhu LIU[1,2*], Guoming GAO[1,2], Guangbo REN[3], Yi MA[3], Jocelyn CHANUSSOT[4] & Xiuping JIA[5]

[1]*School of Electronics and Information Engineering, Harbin Institute of Technology, Harbin* 150001*, China;*
[2]*Heilongjiang Province Key Laboratory of Space-Air-Ground Integrated Intelligent Remote Sensing, Harbin* 150001*, China;*
[3]*First Institute of Oceangraphy, Ministry of Natural Resources, Qingdao* 266061*, China;*
[4]*GIPSA-Lab, Grenoble Institute of Technology, Grenoble* 38402*, France;*
[5]*School of Engineering and Information Technology, University of New South Wales, Canberra* 2610*, Australia*

Received 5 May 2020/Revised 10 August 2020/Accepted 12 October 2020/Published online 21 January 2021

Abstract Since the advent of hyperspectral remote sensing in the 1980s, it has made important achievements in aerospace and aviation field and been applied in many fields. Conventional hyperspectral imaging spectrometer extends the number of spectral bands to dozens or hundreds, and provides spatial distribution of the reflected solar radiation from the scene of observation at the same time. Nowadays, with the fast development of new technology in the fields of information and photoelectricity sensing, and the popularity of unmanned aerial vehicle, hyperspectral remote sensing imaging presents the new trends of multimodality and acquires integration information while keeping high or very-high spectral resolution, especially, high temporal even real time sensing and stereo sensing. Therefore, three important modes of hyperspectral imaging come into existence: (1) multitemporal hyperspectral imaging, which refers to the observation of same region at different dates; (2) hyperspectral video imaging, which captures full frame spectral images in real-time; (3) hyperspectral stereo imaging, which obtains the full dimension information (including 2D image, elevation, and spectra) of observed scene. Along this perspective, firstly, the current researches on hyperspectral remote sensing and image processing are briefly reviewed, and then, comprehensive descriptions of the aforementioned three main hyperspectral imaging modes are carried out from the following four aspects: fundamental principle of new mode of hyperspectral imaging, corresponding scientific data acquisition, data processing and application, and potential challenges in data representation, feature learning and interpretation. Through the analysis of development trend of hyperspectral imaging and current research situation, we hope to provide a direction for future research on multimodal hyperspectral remote sensing.

Keywords hyperspectral image processing, multitemporal hyperspectral imaging, hyperspectral video imaging, hyperspectral stereo imaging, multimodal hyperspectral remote sensing imaging

Citation Gu Y F, Liu T Z, Gao G M, et al. Multimodal hyperspectral remote sensing: an overview and perspective. Sci China Inf Sci, 2021, 64(2): 121301, https://doi.org/10.1007/s11432-020-3084-1

1 Introduction

In 1980s, the Jet Propulsion Laboratory (JPL) first developed Aerial Imaging Spectrometer named AIS-1, then developed AIS-2 and Airborne Visible Infrared Imaging Spectrometer (AVIRIS) with 224 spectral bands range in 0.4–2.5 μm and 9.6 nm spectral resolution [1]. Until now, hyperspectral remote sensing has made important achievements in aerospace and aviation field and applied in many fields such as survey and resource monitoring [2,3], crop yield estimation [4,5], environmental monitoring [6,7], ecological protection [8,9], military defense and security [10,11]. Simply speaking, as shown in Figure 1, hyperspectral remote sensing is to use hyperspectral imaging spectrometer to collect electromagnetic waves, which are separated from each other according to different frequencies by the dispersion prism, and then their energy is recorded in frequency order at some spatial position. Conventional hyperspectral imaging spectrometer can image over some continuous spectral range, and collect data combining image and

* Corresponding author (email: tzliu@hit.edu.cn)

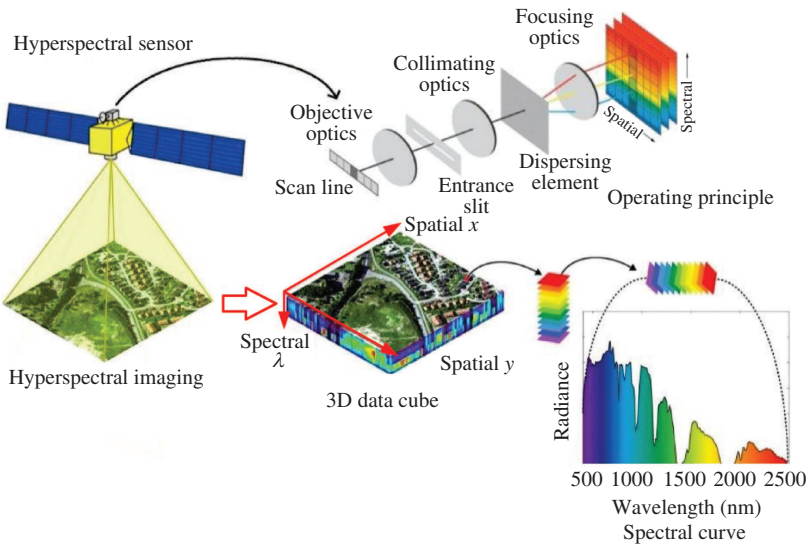

Figure 1 (Color online) Basic principle of hyperspectral remote sensing imaging.

spectrum with higher spectral resolution. The wavelength range of hyperspectral imaging spectrometer is constantly extending, from visible and near infrared, to infrared/thermal infrared, ultraviolet and terahertz spectrum for hyperspectral imaging, which will constitute the full-spectrum imaging pattern with high spectral resolution [12,13]. For example, thermal infrared spectral camera was developed, which can image in infrared bands with high spectral resolution to detect chemical gas [14,15].

As the continuous development of hyperspectral remote sensing, a special issue of *IEEE Signal Processing Magazine* comprehensively and deeply introduced the hyperspectral remote sensing imaging signal processing theory in 2002 [16–20], including corresponding object classification [20], target detection [17, 18] and spectral unmixing [19]. This special issue established the theoretical foundation of researches on hyperspectral remote sensing image processing. This stage mainly involved the application of traditional signal detection theory and pattern recognition in hyperspectral image (HSI) processing. In 2014, another special issue of *IEEE Signal Processing Magazine*, titled *Signal and Image Processing in Hyperspectral Remote Sensing*, reviewed the important research achievements in hyperspectral remote sensing processing field, and pointed out main problems such as nonlinearity, heterogeneity, and sparsity (high dimensionality of hyperspectral data) in the process of hyperspectral signal and image processing. Current researches in aspects of conventional HSI classification [21] and target detection [22,23] mainly involved signal representation-based and machine learning methods. Representation-based methods [24] basically include compressed sensing (CS) [25,26], sparse representation (SR) [27,28], collaborative representation (CR) [29,30] and their extension. For example, joint SR [31–33] and joint CR [34,35] consider the spatial information at neighbouring locations, kernel SR [36,37] and kernel CR [38,39] project the data into a high-dimensional kernel-induced feature space by an implicit nonlinear mapping function. As for machine learning methods, a representative kind is kernel-based methods and support vector machines [40,41]. Especially, multiple kernel learning (MKL) has attracted lots of attention of researchers, which aims at combining a set of basis kernels into a composite kernel [42,43]. A series of MKL methods, such as subspace MKL [44–47], sparse MKL [48–51], ensemble MKL [52,53] and nonlinear MKL [54], have been developed for HSI and other sensor data classification. Manifold learning for HSI analysis [55] has also demonstrated potential value for applications including feature extraction [56,57], segmentation [58], classification [59,60], anomaly detection [61,62], and spectral unmixing [63,64]. Besides, the successful application of deep learning method in HSI classification [65] in 2014 led the wave of deep learning application in HSI interpretation. Since then, a large number of deep learning-based models have emerged [66–70]. Especially, the advances based on mathematical morphology, Markov random fields, segmentation, sparse representation and deep learning in spatial-spectral HSI classification are summarized comprehensively in [70]. More recently, a *Special Focus on Deep Learning in Remote Sensing Image Processing* of *SCIENCE CHINA Information Sciences* has been organized, concentrating on the application of deep learning methods to solve the problems in remote sensing image processing [71–78].

The above *Signal and Image Processing in Hyperspectral Remote Sensing* issue also pointed out new

directions and new challenges in signal processing of HSIs such as object-oriented classification, change detection of multitemporal, multi-angular HSIs with high spatial resolution [21, 55]. Right after that, a special issue concerning on *Multimodal Data Fusion* in multidisciplinary field was organized in *Proceedings of the IEEE* in 2015, which emphasized the urgency and necessity of developing multimodal data fusion [79]. Two papers in this issue were relevant to remote sensing image processing [80, 81], which guided the cutting-edge directions and technologies of multimodal data processing in remote sensing image processing. They focused on two themes, i.e., multimodal remote sensing data fusion and multimodal remote sensing image classification. Multimodal remote sensing image processing was described as a multi-source remote sensing data fusion problem under acquiring conditions with multi-sensor, multitemporal, multi-angular, and multi-resolution. These two papers summarized the important achievements of data fusion, classification and unmixing with multimodal remote sensing data, and pointed out the potential challenges in researches. At the same time, they elaborated the application potentials of new technologies, for example, the aforementioned MKL for feature level fusion [45, 51, 82–86], sparse dictionary learning [87–91], deep learning for multimodal remote sensing image classification [92–95], domain adaptation for alignment of data representations [96, 97]. More recently, some researches have begun to introduce the social media data into the remote sensing [98–101]. Those researches could be treated as general multimodal remote sensing, which focus on how to integrate the social media data to improve interpretation ability of remote sensing data.

After decades of observation platform development, hyperspectral remote sensing is extended from airborne platform into spaceborne platform with large scale of observation, and even unmanned aerial vehicle (UAV) platform with more mobility and flexibility. The multiple model or conditions of hyperspectral data acquisition thus make hyperspectral remote sensing possess the ability to sense with multitemporal, multi-platform, multi-angle and multi-resolution. With the fast progress of new technologies in the fields of information and photoelectricity sensing, at the view of imaging pattern, hyperspectral remote sensing imaging presents new trends of multimodality and acquiring integration information while keeping high or very-high spectral resolution, especially, high temporal even real time sensing and stereo sensing. New ways of hyperspectral imaging generate new types of hyperspectral remote sensing data such as hyperspectral video, stereo hyperspectral point cloud. In other words, multimodal hyperspectral remote sensing is coming. Since hyperspectral remote sensing is growing up from traditional single modality of spectral imaging to new multimodal ways, the spatial-spectral information collected by single modal hyperspectral imaging will be extended in both of time (temporal) and 3-dimensional (3D) spatial dimensions. Such a new kind of multimodal hyperspectral data will be highly complex nonlinear, heterogeneous and sparsity in data representation, feature learning, and interpretation decision.

(1) Nonlinearity. Nonlinearity is a main problem in the conventional hyperspectral remote sensing. The correlation between different bands of HSI is generally nonlinear because of complex classes and spatial distribution of landcovers. This phenomenon will be more serious in the multimodal HSI as its dimension is not only spectra, but also elevation and time. Full dimensions have to be considered while correlation of different bands of multimodal HSI is analysing. That means the correlation measure will be more complex than one in the conventional hyperspectral remote sensing.

(2) Heterogeneity. The full dimension of image, spectrum, elevation and time variables is involved in the multimodal HSI either as whole or as a part. Physical properties and statistical distribution of those dimensions are greatly different. How to full exploit the information complementarity and well handle the heterogeneity will be important.

(3) Sparsity. Past researches had revealed that strong sparsity exists in both spatial and spectral dimension of the conventional HSI. In the multimodal HSI, the more complex nonlinearity and stronger heterogeneity will result in bigger data sparsity. Furthermore, joint sparse structure become high-order and more difficult to be modelled and captured.

In this paper, we try to set forth a new perspective of multimodal hyperspectral remote sensing from the point of imaging detection, and give an overview of relevant data processing as comprehensive as possible. The multimodal discussed in this paper mainly focuses on hyperspectral imaging. In view of the limitations of traditional hyperspectral multi-band imaging, the core of multi-modal hyperspectral imaging is the extension of traditional hyperspectral imaging in temporal and spatial dimensions, i.e., dynamic hyperspectral imaging and hyperspectral stereo imaging. Dynamic hyperspectral imaging includes multitemporal hyperspectral imaging and hyperspectral video imaging. Different from traditional hyperspectral imaging which can only obtain the static information of the scene, the dynamic hyperspectral imaging aims at obtaining the time-varying information of the observed objects. As for hyperspectral

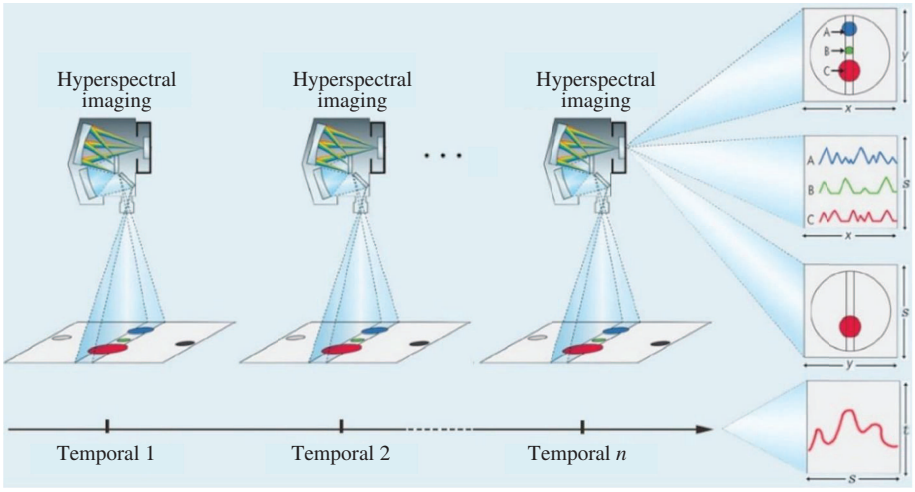

Figure 2 (Color online) Multitemporal hyperspectral imaging.

stereo imaging, it is different from the traditional hyperspectral imaging in the process of which the elevation information degenerates, it can obtain 3D spatial information and spectral information simultaneously. Thus, the observed real object in remote sensing scene can be described by full dimension of 2D image, elevation, and spectra. Starting with a brief review of traditional HSI processing (Section 1), new types of hyperspectral remote sensing imaging, including multitemporal hyperspectral imaging (Section 2), hyperspectral video imaging (Section 3) and hyperspectral stereo imaging (Section 4), are presented from the following four aspects one by one: fundamental principle, data acquisition, processing and applications and major issues in data processing. Finally, conclusion is drawn in Section 5.

The main contribution of this paper mainly has three aspects: (1) The meaning of each new type of hyperspectral remote sensing imaging has been defined. (2) Typical models dealing with multimodal hyperspectral remote sensing data have been reviewed detailedly. (3) The major issues in multimodal hyperspectral remote sensing data processing have been summarized, which lead the way of follow-up research.

2 Multitemporal hyperspectral imaging

2.1 Fundamental principle

Multitemporal hyperspectral imaging refers to the observation of same region at different dates. It is designed to utilize the different hyperspectral information obtained at different times for remote sensing applications. Temporal variable is an important dimension of remote sensing information acquisition. Temporal-varying spectrum and spatial distribution are of great significance to study change detection of landcovers and explore its temporal and spatial change pattern. The existing multitemporal remote sensing imaging mostly refers to multispectral images (MSIs) with high spatial resolution, but the spectral resolution is very low. Compared with the existing multitemporal multispectral remote sensing, multitemporal hyperspectral imaging with better temporal resolution and higher spectral resolution will play more and more important role in precise classification and change detection. Multitemporal hyperspectral images (MultiTemp-HSIs) can be seen as the continuous extension of hyperspectral data in the temporal dimension. It means that the description of the data from the image and spectrum dimension (x-image, s-spectrum) in the original hyperspectral space is extended to higher dimension (x-image, s-spectrum, t-temporal space). Figure 2 shows the principle of multitemporal hyperspectral imaging.

2.2 Data acquisition

Current ways of multitemporal hyperspectral data acquisition mainly include two kinds: spaceborne and airborne multitemporal hyperspectral acquisition. Spaceborne MultiTemp-HSIs are mainly collected by the existing hyperspectral sensors boarded on satellites or the space station observing same area at different time. Spaceborne hyperspectral sensors boarded on satellites mainly conclude EO-1 Hyperion of

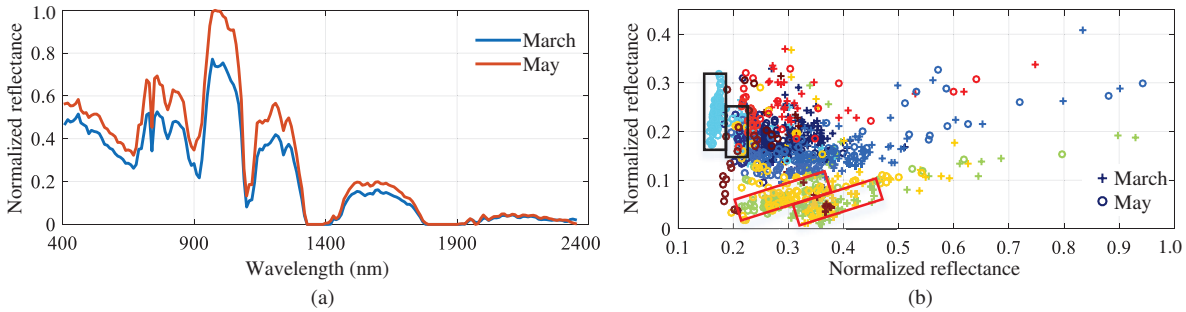

Figure 3 (Color online) Spectral drift in bi-temporal HSIs obtained by the same sensor. (a) The spectrum of the same class in bi-temporal HSIs; (b) scatter diagram of bi-temporal HSIs.

America, PROBA CHRIS of Europe, ARIES-1 of Australia, GF-5, Zhuhai-1 satellite constellation, and Tiangong-1 (TG-1) and Tiangong-2 (TG-2) hyperspectral sensors boarded on space station of China. Airborne MultiTemp-HSIs are acquired by multiple repetitive flights with manned fighter or unmanned aerial vehicle (UAV) equipped with hyperspectral sensors (such as AVIRIS). The spaceborne multitemporal hyperspectral imaging has many advantages such as wide range of observation, more data sources, stable imaging conditions, and mature processing methods.

2.3 Processing and applications

There are three major applications in MultiTemp-HSI processing: multitemporal classification, multitemporal change detection and multitemporal spectral unmixing. Multitemporal classification has attracted extensive attention of researchers, while there are relatively few studies on multitemporal change detection and multitemporal spectral unmixing.

2.3.1 *Multitemporal classification*

Multitemporal classification is defined to train a classifier with one (or several) remote sensing data set and perform classification task on another data set collected at different dates. Main scientific problems with the MultiTemp-HSI classification can be mostly categorized into spectral drift and spectral mismatch.

Spectral drift means that spectral variation exists in the data collected by the same sensor at different date. Most researches focused on the case that the MultiTemp-HSIs are collected by the same sensor. Under this condition, main problem confronted with multitemporal classification is spectral drift (also called spectral variation) of the HSIs collected at different dates, caused by different observation conditions such as illumination, atmosphere, and natural evolution of the scene. Figure 3 shows the spectral drift in bi-temporal HSIs obtained by Hyperion on the NASA EO-1 satellite over Brookings in March and May of 2011. Figure 3(a) shows the spectrum of the same class in bi-temporal HSIs. Figure 3(b) exhibits the scatter diagram of bi-temporal HSIs, where different shapes mean bi-temporal HSIs obtained by the same sensor over the same geographical area, and different colors denote different land cover types. There exists an obvious drift in spectral signatures of light blue category from bi-temporal HSIs in the black boxes, so does the spectral signatures of yellow category and green category in the red boxes.

Many methods have been developed in the past decades to address the aforementioned problem. Previous studies such as linear regression [102, 103], nonlinear image normalization [104], nonlinear histogram shape matching [105] and multidimensional histogram matching [106] have been done, which focus on making the statistical properties of image pair similar to each other. Some of multitemporal classification adopted strategies such as combining evidence theory [107, 108], texture information [109] and multi-classifier decision fusion system [110]. In some researches, multitemporal classification was achieved by knowledge transfer [111]. For example, in [112], a feature-level domain adaptation technique based on dictionary learning was proposed, which maps the spectral features of the source and target HSIs into a common low-dimensional embedded space through multi-task dictionary learning, so as to align the spectral feature distribution between the bi-temporal hyperspectral data. Laplacian support vector machines (LapSVM) method was proposed in [113] for solving spectral drift, in which the classifier in LapSVM was adapted to the new data set via iterative application of the classifier using the clustering condition on the data manifold. In addition, in order to realize the classification of MultiTemp-HSIs, Yang and Crawford [114] used spatial information of HSIs to regularize the solutions of manifold alignment (MA) and

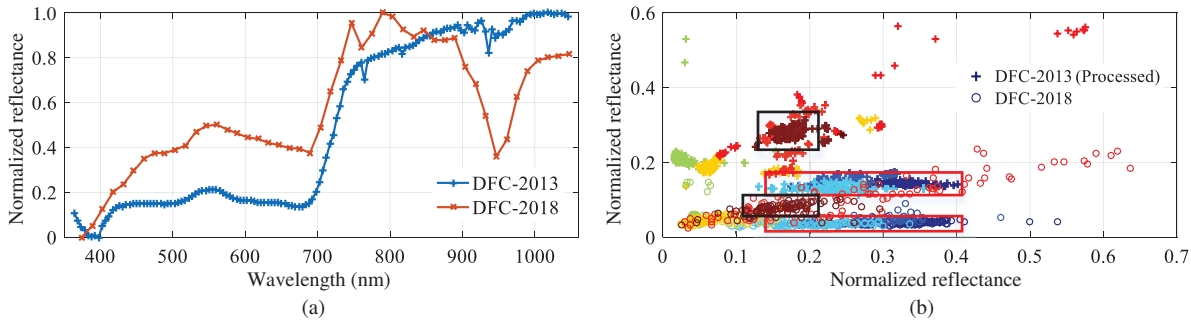

Figure 4 (Color online) Spectral mismatch in bi-temporal HSIs obtained by different sensors. (a) Spectrums of the same category obtained by different sensors; (b) scatter diagram of bi-temporal HSIs obtained by different sensors.

obtained more stable and portable feature representation. They further proposed a multi-scale method based on clustering pairs instead of marking instances, and considered the retention of local and global geometric features [115]. Subspace alignment (SA), such as principle component analysis (PCA) and kernel PCA [116], canonical correlation analysis (CCA) [84] and semi-supervised kernel CCA [117], transfer component analysis (TCA) [97, 118], geodesic flow kernel (GFK) [119], is also a typical kind of method used for overcoming spectral drift. It maps data into common latent space or into different subspaces and then builds connections between them. By extending the subspace method to tensor space, the tensor alignment method [120–122] has also been successfully applied to multitemporal remote sensing image classification to solve the spectral drift problem. Besides, there are also methods such as active learning [123], graph-matching [124, 125], hidden markov random fields [126], 3D spectral modeling [127, 128], pre-processing or compensating for differences in lighting conditions, transforming spectral signatures and atmospheric effect [107, 129]. Recent years, deep learning methods become a research hotspot and has been successfully applied in multitemporal classification [130–132].

Spectral mismatch means that spectral variation exists in the data collected by different sensors. In practice, MultiTemp-HSIs can also be collected by different hyperspectral imaging sensors. Under this circumstance, except the spectral drift, different parameters of sensors will cause a new problem, i.e., spectral mismatch. Spectral mismatch is mainly embodied in the difference of spectrum range, spectral resolution, central wavelength and number of spectral bands. Figure 4 demonstrates the spectral mismatch in bi-temporal HSIs obtained by different sensors. The bi-temporal HSIs were collected by different hyperspectral imaging sensors over the University of Houston, and were released at IEEE GRSS Data Fusion Contest (DFC) in 2013 and 2018. As exhibited in Figure 4(a), the acquired spectrums of the same category from the bi-temporal HSIs are inconsistent. Although DFC-2013 can be down sampled to obtain the same spectral resolution and band number as DFC-2018, central wavelengths of the processed DFC-2013 and original DFC-2018 are still discrepant, so that the distribution of spectral features of the bi-temporal HSIs is significantly different, which can be seen in Figure 4(b), especially for the categories in the black boxes and in the red boxes, respectively. In this case, multitemporal classification based on only spectral features can be relatively difficult.

So far, by our survey, there are few studies focusing on spectral mismatch. Semi-supervised manifold alignment [96, 133] and its kernel extension [134] ensure the proximity of the intrinsic structure of manifolds in the alignment space by using labeled samples in each temporal, meanwhile, unlabeled samples are also introduced into the preserving of manifold structure by using the graph method, realizing the collaborative classification of heterogeneous multimodal remote sensing data. In [135], a supervised classification method is proposed based on sparse subspace correlation analysis. This approach is not limited by data dimensions or data acquisition sensors, and can learn the sparse representation of heterogeneous data in source and target domains in potential common subspace, so as to realize the transfer learning between hyperspectral remote sensing images. In [136], a heterogeneous domain adaptation method was proposed which utilizes the limited samples of hyperspectral data from both source domain and target domain. This method adopts the method of cross-domain collaborative learning, which is realized by cluster canonical correlation analysis and random walker algorithm. Aiming at achieving accurate land cover classification over a large coverage based on the large coverage MSI and locally overlapped HSI, a cross-modality feature learning framework is proposed which learns the common subspace from hyperspectral-multispectral correspondences [137].

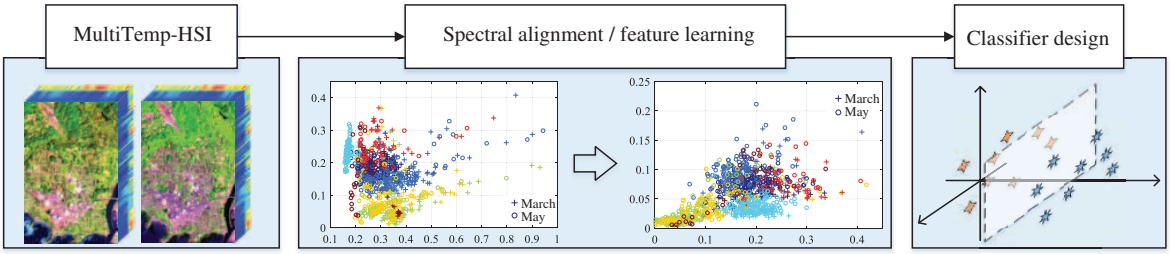

Figure 5 (Color online) General flowchart of multitemporal classification.

According to the above review of current research, general processing steps of multitemporal classification can be summarized to two main stages as shown in Figure 5, the first step can be boiled down to spectral alignment or feature learning to make the original features form source and target domain lie in the same feature space, and the second step is classifier design to discriminate the classes accurately. However, the problem is that, most of these studies do not take the spatial information into consideration. In [138], a cross-temporal spatial-spectral classification method of HSIs obtained by different sensors is proposed, namely spatial-spectral multiple geodesic flow kernel learning (S2-MGFKL). Since the bi-temporal HSIs are captured over the same geographical area, the authors conclude that spatial features must be useful in the transfer process. Based on the general framework of multitemporal classification, spatial feature extraction and alignment steps are added in the framework of S2-MGFKL method. The whole process can be simply understood as firstly constructing geodesic flows (GFs) with each pair of the corresponding features from the source and target domain, and then designing different kernel scale selection schemes respectively for the spectral and spatial features to generate Gaussian MGFKs. Specifically, each pair of spatial or original spectral features from both domains is used to construct the GFs, and then, mapping matrices can be obtained which projects the spatial and spectral feature pairs of MultiTemp-HSIs to the domain-invariant feature spaces [139]. For the original spectral feature pair, multiple spectral Gaussian GFKs can be built by tuning the kernel scales. For each spatial feature pair, a spatial GF and a corresponding mapping matrix can be obtained. Based on them, the spatial Gaussian MGFKs can be constructed whose kernel scales are the same. Note that, the spatial features can be extracted by the filters of various degrees, and thus one does not need to tune the kernel scales of spatial MGFKs. All the S2-MGFKs can be combined by any MKL methods and input into SVM to complete the domain transfer classification task.

Experiments are conducted on two datasets. Brookings dataset contains three HSIs collected by Hyperion over Brookings, USA. Houston dataset contains two HSIs acquired over the University of Houston campus and the neighboring urban area by different sensors. In each dataset, an arbitrary HSI is selected as the source image to classify another image (target image). The experimental results clearly show that the S2-MGFKL framework can achieve the highest classification accuracy for almost all the data pairs, which proves its validity. For Brookings dataset, the classification accuracies have been improved by 2%–9%, which demonstrates that S2-MGFKL model can deal with the spectral drift problem. For Houston dataset, the classification accuracies have been increased by more than 15%. Significant improvement has been gotten, while the compared methods cannot perform well, which not only demonstrates the validity of integrating the spatial features to enhance the domain adaptation effect of S2-MGFKL model, but also demonstrates the proposed S2-MGFKL model can deal with the spectral mismatch problem.

2.3.2 *Multitemporal change detection*

Except for multitemporal classification, multitemporal change detection is another hot topic of researches on MultiTemp-HSI processing. Multitemporal change detection is to find out changed and unchanged landcovers, using hyperspectral data collected at different dates but over the same geographic area. As shown in Figure 6, current studies on multitemporal change detection can be devised into two kinds: common feature extraction-based methods which can weaken the influence of imaging condition change on the spectrum in the process of feature extraction, and post-classification methods which detect the multiple changes by comparing the difference between classification results. Liu et al. [140,141] proposed and extended hierarchical change detection approaches, and they also explored detecting multiple changes. Cesmeci et al. [142] integrated spatial and spectral processing into the change detection process. Some

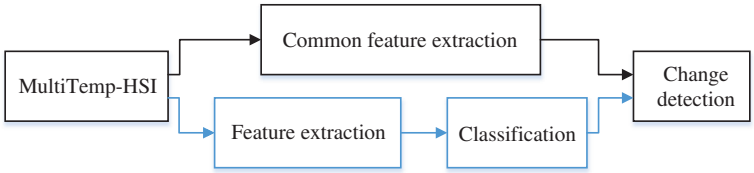

Figure 6 (Color online) General flowchart of MultiTemp-HSI change detection.

change detection methods aim at finding change residuals in unsupervised way, for example, slow feature analysis (SFA) [143] and deep SFA [144], and in semi-supervised way [145]. Another operation aims at detecting change of stacked MultiTemp-HSIs [146]. Object-level change detection (OLCD) [147] and scene-wide change detection methods [148] have also been presented. Partial change detection algorithms such as multivariate alteration detection (MAD) were also applicable for radiometric normalization, which is often an important pre-processing procedure for change detection [149].

2.3.3 *Multitemporal spectral unmixing*

The spatial resolution of HSIs are generally low, so that spectral unmixing is required. Recent studies are particularly interesting examples of fusion, as multiple (spatial, spectral, temporal) information modes are jointly considered by exploiting the possibilities offered by MultiTemp-HSIs [81]. Halimi et al. [150] analyzed spatial-temporal endmember variability under a Bayesian framework. Thouvenin et al. accounted for both smooth and abrupt variations [151] and introduced them into an online estimation algorithm for saving computation memory [152, 153]. Henrot et al. [154] proposed a dynamical model to reduce computational complexity. Licciardi et al. [155] applied neural networks (NNs) for solving the unmixing problem. Besides, some researchers investigated unmixing techniques for change detection [156,157], with sparse techniques [158, 159] and superpixel to integrate the spatial information. Spectral unmixing can also be applied to seasonal change analysis and cloud removal [160, 161].

2.4 Major issues in data processing

There are two major issues in MultiTemp-HSI processing.

(1) Multi-dimension alignment of MultiTemp-HSI. The spectral drift is confronted by all MultiTemp-HSI processing including classification, change detection and spectral unmixing. The spectral mismatch is also an intractable issue if the MultiTemp-HSIs are acquired by different sensors. To achieve MultiTemp-HSI processing, one must implement multi-dimension alignment to overcome the spectral difference caused by varying acquisition conditions, which include not only illumination, atmosphere condition and angle of view, but also spatial resolution, spectral band setting, and even natural evolution of the scene. Besides, compared to MultiTemp-MSI, high dimensionality, nonlinearity, and coupling of different dimensions will be more serious in MultiTemp-HSI, leading to more troublesome multi-dimension alignment.

(2) Multilevel change detection. Most of the current researches are focused on how to detect changes. This can be treated as the first level in fine change detection. More details about the changes are necessary in many remote sensing applications. For example, how many and which classes have changed (changed classes), what classes they have changed to (types of changes), and the speed of changes (i.e., fast or slow changes of these classes). Fine spectral resolution in MultiTemp-HSI will enable the aforesaid appeal of change detection at different levels and different scales. Furthermore, evolution law could be figured out by the multilevel change detection. To achieve the multilevel change detection, new theories and methods should be developed as soon as possible.

3 Hyperspectral video imaging

3.1 Fundamental principle

Traditional hyperspectral imaging spectrometers have to confront a tradeoff between spatial, spectral and temporal resolutions, which generally capture data at low temporal resolution from airborne or spaceborne platform. The traditional hyperspectral remote sensing is not suitable for monitoring dynamic scene in a real-time or near real-time way, although it has been used to observe scene with spatial imagery and high spectral resolution, such as object classification, object detection and change detection. Recent advances

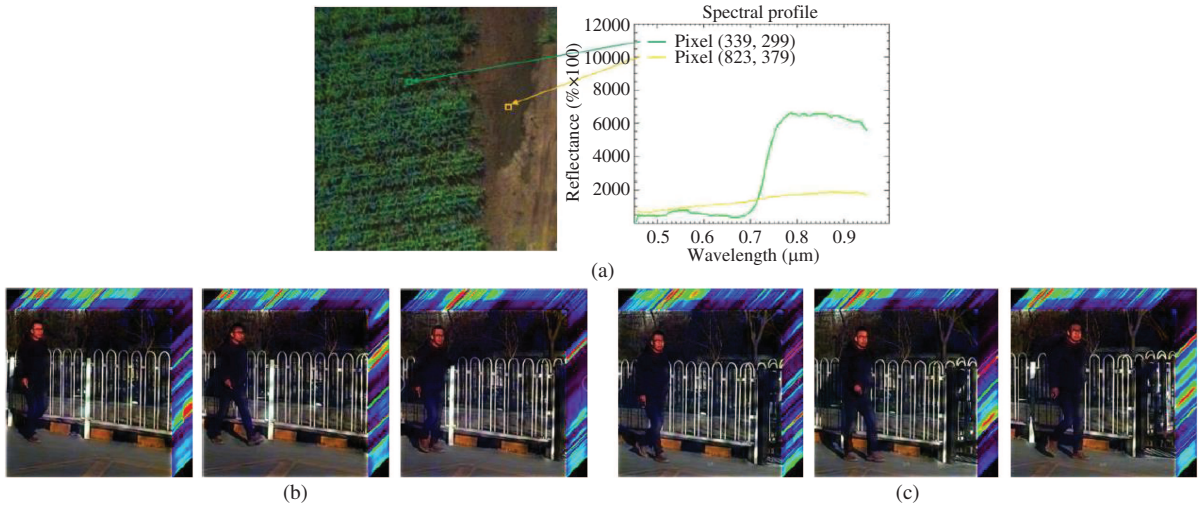

Figure 7 (Color online) An example of HSV data. (a) False color image of HSV and spectral profiles of grass and soil; (b) frames 1–3 in the 1st second; (c) frames 1–3 in the 2nd second.

in electronic and sensor design have enabled the development of HyperSpectral Video (HSV) spectrometer, which can capture full frame spectral images in real-time. It is especially useful for measuring fast and transient phenomena. As defined in [162], HSV camera can get dozens of hyperspectral data cubes per second. HSV can provide important time-varying information of image and electromagnetic spectrum for the dynamic monitoring of interested objects in the scene. Figure 7(a) shows the false color image of HSV at a moment (left) and the corresponding spectral profiles of grass and soil (right), Figures 7(b) and (c) exhibit some continuous frames in an HSV.

3.2 Data acquisition

At present, UAV platform-based near real-time hyperspectral video spectrometer has been developed abroad. American Bodkin Design & Engineering (BD&E) company designed two VNIR video hyperspectral imaging systems. One is VNIR-20B with 1280×1024 CCD imaging area array, which can provide images with 180×180 pixels and 20 bands range in 425–675 nm. The other is VNIR-90 with less pixels with 53×34, but it can provide images with 90 bands whose wavelengths range in 500–900 nm. German Cubert Company designed a frame based non-scanning and real-time imaging spectrometer, which perfectly combined spectral accuracy of the spectrometer and fast camera imaging speed. Its unique design principle is to guarantee the easy access to HSI and obtain real-time video HSI data as well. Canadian TELOPS Company showed that the infrared hyperspectral imager can be applied to monitor chemical gas emission and dynamic monitoring. Other companies and institutes such as Surface Optics (SOC), HySpex, and Specim have also developed their HSV spectrometers.

3.3 Processing and applications

As a new imaging pattern, HSV can capture HSI in real-time or near real-time way, which can provide important change information of target of interest with respect to spatial and temporal domain. HSV will play a critical role in the fields where the temporal resolution is highly required, such as disaster response to oil spills, chemical gas plume detection [14], medical diagnosis [163] and military operations.

HSV can be used to solve computer vision tasks with high temporal, spectral and spatial resolution. At present, HSV interpretation mainly focuses on target behavior trajectory analysis, and the workflow is displayed in Figure 8, which contains three stages. The last two steps are the most critical: HSV feature extraction mainly contains key frame extraction, static and dynamic feature extraction; while the target behavior trajectory analysis basically refers to target detection, recognition and tracking. In [164], the results showed that the HSV was combined with traditional algorithms to achieve illumination-invariant motion detection and object tracking in video surveillance. Considering several challenging conditions, in [165], a framework that combined spectral detection and mean shift algorithm was proposed to track pedestrians in HSVs. The results showed good robustness against abrupt motion and rapid illumination changes. It can be seen that HSV is superior to RGB video because of its fine spectral information.

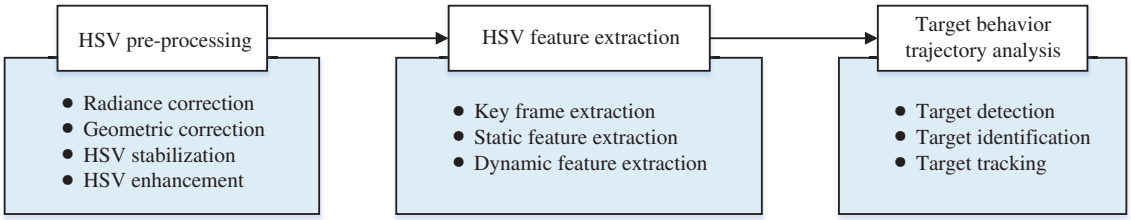

Figure 8 (Color online) General flowchart of HSV interpretation.

In [166], the research work showed the properties of several hyperspectral imagers from visible through the long wave infrared (LWIR), which have been developed by BD&E. They used the VNIR hyperspectral systems to demonstrate tracking of objects and vehicles based on their spectral signatures over time.

In addition, the medium wave infrared (MWIR) hyperspectral system is used to measure and identify the invisible chemicals gas plume. The detection of chemical plumes is significant for many applications such as trace-gas emissions, environmental protection, and disaster response. The HSV data have been gradually applied for the gas plume detection problem, which can capture the potentially invisible gas plume. The published benchmark HSV sequence data sets were provided by Applied Physics Laboratory at Johns Hopkins University. The sensors capture the data cube every five seconds with 129 bands whose wavelengths range from 7.83 μm to 11.7 μm in the LWIR domain. The spatial dimension of each data is 128×320 pixels. There are several researches on the two benchmark data sets. Some methods focus on gas target and background separation based on spectral clustering. In [14], PCA was used to reduce the dimension of the entire video sequence at first, and then Midway method was used for histogram equalization. Finally, K-mean, spectral clustering, and MBO were used to segment the chemical plume. Analogously, clustering methods were adopted for classification, where the graphical MBO scheme was used to track and classify objects in HSV [167,168]. The pixels of the images in the video were considered as vertices in a graph, and then Nystrom was used to quickly approximate the Eigen-functions of the graph Laplacian. For the gas tracking methods based on infrared HSV, they can be roughly divided into three categories according to their basic principle: tracking method based on spectral unmixing [154,169], tracking method based on low-rank representation [170–172] and other related methods based on image decomposition [15,173]. In [170], the authors proposed a low rank representation model for gas plume detection. It assumed that each frame of HSV can be decomposed into a low-rank and a sparse term, corresponding to the background and the plume, respectively. The temporal consistency was incorporated by adding a residual regularization. In addition, the total variation was added to smooth the gas plume in spatial domain. Furthermore, they proposed a gas tracking method based on low-rank decomposition of HSV and constraint of overall spatial and temporal variation [171]. Tochon et al. [15] introduced research results for gas plume detection by hyperspectral video sequences. The temporal redundancy was used to estimate the location of the plume, and then a binary partition tree was built to retrieve the real location and extent of the plume in the frame. After that, the work was extended in [173].

However, the processing stage of most aforementioned methods is based on independent pixels or single-band images. In order to achieve sufficient use of sequential 3D information and inter-frame information, a sequential tensor decomposition (STD) method for gas tracking is proposed, where a series of 3D tensors are used to represent HSV [174]. It is assumed that the static background in adjacent frames has a low-rank property, and therefore, low rank tensors can be used to approximate the background. However, the moving gas plume cannot satisfy the low-rank hypothesis, and thus it can be expressed by the obtained error tensors. The STD method uses the obtained low-rank tensors to reveal the gas target in the whole HSV, so as to track the gas. Let $\mathcal{X}^t$ denote a frame of HSI obtained at time t, it is a 3-order tensor and can be decomposed into low-rank tensor $\mathcal{A}^t$ corresponding to the background and error tensor $\mathcal{E}^t$ corresponding to the target, that is, $\mathcal{X}^t = \mathcal{A}^t + \mathcal{E}^t$. The decomposition problem of single 3D tensor $\mathcal{X}^t$ can be expressed as

$$\min_{\mathcal{A}^t_{(n)},\mathcal{E}^t_{(n)}} \sum_{n=1}^{3} \left(\frac{1}{2} \left\| \mathcal{X}^t_{(n)} - \mathcal{A}^t_{(n)} - \mathcal{E}^t_{(n)} \right\|_F^2 + \lambda_1 \left\| \mathcal{A}^t_{(n)} \right\|_* + \lambda_2 \left\| \mathcal{E}^t_{(n)} \right\|_1 \right), \tag{1}$$

where $\|.\|_F$ denotes the Frobenius norm of a matrix, $\|\mathcal{A}^t_{(n)}\|_*$ and $\|\mathcal{E}^t_{(n)}\|_1$ denote the nuclear norm and l_1 norm of mode-n unfolding matrix $\mathcal{A}^t_{(n)}$ and $\mathcal{E}^t_{(n)}$, respectively. λ_1 and λ_2 are regularization parameters

for low-rank and sparsity error components. By introducing the dictionary $\boldsymbol{D}_n^t$, $\mathcal{A}_{(n)}^t$ can be replaced by the matrixed result of the sparse coding of it, while $\boldsymbol{D}_n^{t-1}$ can be updated to $\boldsymbol{D}_n^t$ for time t, considering that the background components in adjacent frames are similar to each other. Finally, the outputs $\mathcal{A}^t$ and $\mathcal{E}^t$ are obtained by converting the corresponding $\mathcal{A}_{(n)}^t$ and $\mathcal{E}_{(n)}^t$ to tensors in all three dimensions and computing their mean.

In the experiment, the HSV was collected over the scene where the target gas, sulfur hexafluoride, was being emitted. This HSV consists of 60 frames of infrared HSIs with 128×130 pixels and 127 spectral bands range from 7.8 μm to 11.8 μm. Compared with several traditional tracking methods, the tracking results produced by STD method are colorredthe clearest and most similar to the ground truth, while the receiver operating characteristic (ROC) curve corresponding to tracking result of each frame is also the closest to the upper left corner. This STD method achieved relatively good results, because it can not merely take full advantage of the entire information in each frame, but also consider the background similarity among all the frames.

3.4 Major issues in data processing

There are three major issues in HSV processing.

(1) HSV data modelling. The HSV data are dynamic hyperspectral data cubes and will be very different from the traditional static hyperspectral data. The difference lies not only in the increment of data amount, but also in HSV data's high-dimensionality and heterogeneity of time, spectral and spatial dimensions. Therefore, the first issue of HSV data processing is to model the complex high-order data.

(2) HSV feature learning. HSV can provide fine spectral resolution to represent the observed scene compared with most of modern videos. Therefore, spectral properties must be incorporated when traditional video processing techniques are extended to perform tasks of HSV, such as object detection and tracking. There are many challenging conditions, such as variations of illumination conditions, rapid movements and different reflectance properties of the objects in the scene. The high-resolution spectral features can be used to distinguish the tracked objects according to different reflectance properties of objects, and also help in building the connection of different temporal, spectral and spatial dimensions of the objects to be tracked. Therefore, learning effective and discriminative features from HSV will be important and challenging.

(3) Benchmark HSV data set construction. Benchmark HSV data sets are very rare in science research, and it is difficult to quantitatively evaluate novel methods owing to lack of ground-truth data. However, ground-truth data are difficult to determine even by survey and expert knowledge at cost of material resources and manpower, especially in the face of large data volume and complex scene. Therefore, more benchmark HSV data sets and corresponding ground-truth data are needed for science research.

4 Hyperspectral stereo imaging

4.1 Fundamental principle

The existing hyperspectral imaging detection can simultaneously obtain spatial distribution and spectral information of interested objects in narrow band range with high spectral resolution. However, the traditional hyperspectral remote sensing has to confront information loss in both of spatial and spectral dimension. It is well known that the observed object in a scene is actually in the 3D space. Therefore, the real 3D object is degraded to be 2-dimensional (2D), i.e., image, in the imaging process. In this case, the depth (or height, elevation) would be degraded or even lost. Correspondingly, the spectra of the objects is also not real, but comes from the degraded 2D images. In other words, the observed real object in remote sensing scene should be described by full dimension of 2D image, elevation, and spectra.

HyperSpectral image and elevation (HSE) is a new type of remote sensing data which can meet the above requirement, as shown in Figure 9. It is obtained by newly developed hyperspectral imaging spectrometer, which is designed to acquire such a full dimension of static hyperspectral data. For example, multispectral LiDAR and hyperspectral LiDAR can get multiband point clouds and provide full information of images, elevation and spectra. The hyperspectral LiDAR combines the three dimensional, active, and foliage penetrating capabilities of monochromatic LiDAR systems with the spectral imaging capability of hyperspectral imaging sensor. As a novel active remote sensing technique, HSE system offers the potential to directly provide spectral information for each recorded 3D point, independent of

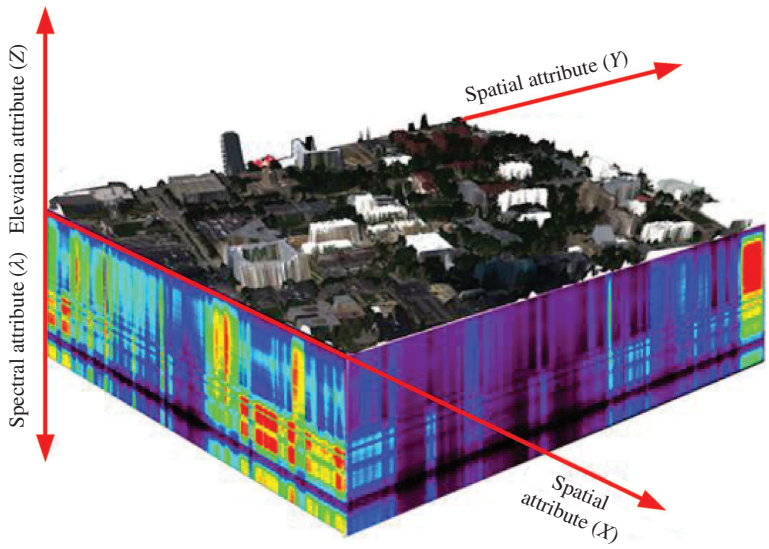

Figure 9 (Color online) HSE: a full dimensional hyperspectral imaging.

solar illumination. Since the geometry and spectral information of the target can be obtained by a single measurement, this technology will extend the scope of imaging spectrometer into 3D spectral sensing.

HSE has obvious advantages over the fusion of passive spectral data with structural information of monochrome LiDAR. First and foremost, since the instantaneous field of view (IFOV) of the laser pulse is relatively small, the spectrum of each point is independent of any other point along the point ray, and the spectral mixing within each measured point cloud is minimal. Secondly, since LiDAR can detect multiple targets in a single point cloud ray, which will partially block the transmission beam in a single transmission, the spectrum of each echo is range resolved. The fusion of passive spectral images with monochromatic LiDAR images cannot achieve this, because the pixels of the passive sensor are not range resolved and will irreversibly mix the spectra of the constituent block voxels, possibly mounting the perspective error in the process. Next, owe to the active property of HSE, the spectrum is unaffected by illumination conditions such as shading, uncertain vertical atmosphere, or secondary scattering effect. In addition, HSE's ability to operate day and night solves the problem of passive hyperspectral imaging at night. Last but not least, registration between the spectral and elevation information is not required.

4.2 Data acquisition

To obtain HSE data, three ways will be available recently and in near future. First, some prototype systems of multispectral LiDAR and hyperspectral LiDAR have been developed, which can be treated as multiband imaging LiDAR (M-LiDAR). The multi-/hyper-spectral LiDAR gets the point clouds and the corresponding intensity images at different wavelengths. Those multiband point clouds can be registrated and combined either as a false color point cloud or to jointly use for object interpretation. Supercontinuum laser source can produce directional broadband light by making using of cascaded nonlinear optical interactions in an optical fiber [175]. The commercial availability of supercontinuum laser technology has led into a number of applications in recent years. Among them, the HSE is a representative product [176]. In contrast to passive remote sensing systems that rely on reflected solar radiation, HSE utilizes its own active white light source generated by a supercontinuum laser source to measure the 3D location (x, y, z) on the surface of the object, and measures the return intensity of different wavelengths through diffraction grating. HSE images the environment by explicitly associating a vector in spectral space with each vector in 3D world space, and produces a 3D point cloud with hyperspectral laser return intensity (LRI): $(x, y, z, R(\lambda))$, where $R(\lambda)$ is the laser return intensity as a function of the wavelength λ.

The second way is to generate the full dimension of HSE data by data alignment. By means of data processing algorithms, HSE data can be generated with separate hyperspectral data and LiDAR point cloud.

The third way is to develop integrated hyperspectral LiDAR system. The integrated hyperspectral LiDAR (Int-Hyper-LiDAR) aims to get the hyperspectral point cloud at once. This kind of hyperspectral

Figure 10 (Color online) UAV multispectral LiDAR system.

LiDAR data will include only one point-cloud, but each point will have spectral information. The data will be real 3D spectra.

At the very beginning, the response of multispectral LiDAR was simulated by using monochromatic LiDAR data based on assumptions about material distribution and spectra [177]. A measurement system, which is composed of a spectrometer, a cutting-edge technology, white-light supercontinuum laser source and a commercial monochromatic LiDAR system, was presented to produce a virtual hyperspectral LiDAR dataset by fusing the backscattered reflectance spectra and distance information [178]. For the past few years, several prototypes of multispectral or hyperspectral LiDAR systems have been developed, which are mainly laboratory based. The University of Edinburgh has demonstrated for the first time a multispectral LiDAR with four wavelengths (531, 550, 660 and 780 nm) that can be used for detailed structural and physiological measurements of forest ecosystems [179]. Heriot-Watt University designed another four-wavelength prototype multispectral LiDAR system (531, 570, 670 and 780 nm) [180]. Intending for the remote sensing of vegetation reflection, a four-laser multispectral canopy LiDAR system (555, 670, 700 and 780 nm) was designed [181]. The Finnish Geodetic Institute (FGI) exploited and constructed the first prototype of a full waveform terrestrial HSE, which can measure 3D point clouds included with eight-channel hyperspectral backscattered reflectance (542, 606, 672, 707, 740, 775, 878 and 981 nm) for each point [182]. The first operational multispectral airborne laser scanning (ALS) system with three channels (532, 1064 and 1550 nm) was launched by Teledyne Optech (Ontario, Canada) in late 2014 with the product name Titan [183]. Each channel produces a separate point cloud, and multispectral intensity values are not originally available for single points. Preprocessing procedure is thus needed before the multispectral information can be utilized.

A new set of UAV multispectral LiDAR system has been implemented in [184] with the support of National Natural Science Foundation of China, which belongs to the second data acquisition approach. The main sensors of this system are LiDAR detectors and multispectral cameras, which are stably fixed and mounted on the UAV using a rigid framework, as shown in Figure 10. Synchronous data acquisition of LiDAR and multispectral camera is realized by a synchronous pulse trigger, so that the system can acquire 3D point cloud and 2D MSI simultaneously. Then, multi-/hyper-spectral point cloud data can be obtained by spatial consistency sampling and multidimensional integrated data generation. To the best of our knowledge, this is the first multi-dimensional information remote sensing detection system which integrating multispectral camera and LiDAR on an UAV platform.

In order to verify the actual performance of the system, field data acquisition experiments were carried out in three places using the developed UAV platform based spectral-stereo imaging detection system, as shown in Figure 11. The first place is Gurigesitai National Nature Reserve in West Wuzhumuqin Banner in Xilin Gol League, Inner Mongolia Province (central geographic coordinates: 118.713799°E, 44.485341°N), where the main species of vegetation include Artemisia Frigida Willd, Chinese wild rye, and achnatherum splendens. The second place is Yellow River Delta National Nature Reserve in Dongying, Shandong Province (119.068910°E, 37.816394°N), where the main species of vegetation include Tamarix Chinensis, Suaeda salsa, and Spartina Alterniflora. The last place is Shankou Mangrove National Ecology and Nature Reserve in Beihai, Guangxi Province (109.760954°E, 21.497706°N). The species of mangrove include Avicennia Marina, Rhizophora Stylosa, and Bruguiear Gymnorrhiza. Taking the experimental area of the Shankou Mangrove National Ecology and Nature Reserve as an example, the relevant data

(a) (b) (c)

Figure 11 (Color online) Field test area. (a) Gurigesitai National Nature Reserve; (b) Yellow River Delta National Nature Reserve; (c) Shankou Mangrove National Ecology and Nature Reserve.

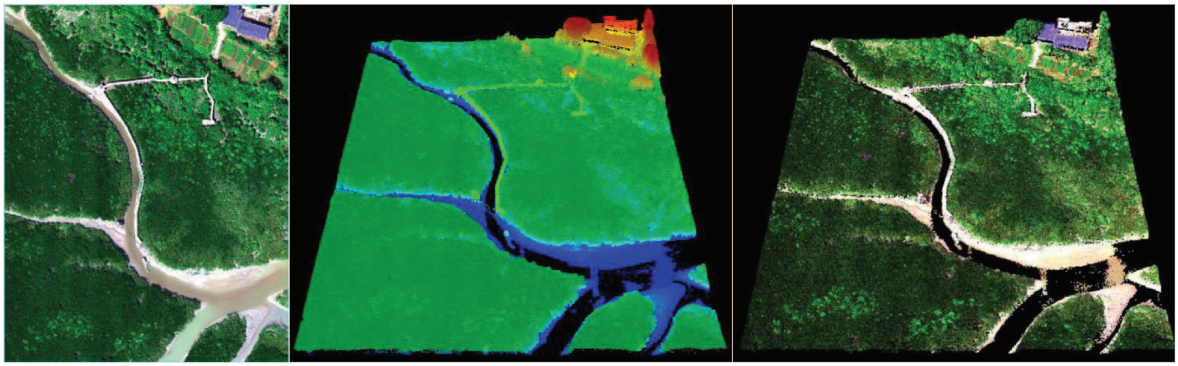

(a) (b) (c)

Figure 12 (Color online) Field test data of Shankou Mangrove National Ecology and Nature Reserve. (a) MSI (false color); (b) LiDAR point cloud; (c) stereo multispectral point cloud.

collected are shown in Figure 12, in which Figures 12(a)–(c) are respectively MSI (false color), LiDAR point cloud and stereo multispectral point cloud data (spectrum-spatial 3D integrated data).

4.3 Processing and applications

When it comes to HSE data processing, joint utilization of multi-/hyper-spectral images and LiDAR data have to be mentioned. Before the integrated HSE data can be obtained, joint utilization of multi-/hyper-spectral images and LiDAR data were widely studied, which aims at overcoming the problem of information loss in the data acquisition process of single sensor, so that more accurate interpretation of observed scene can be obtained.

4.3.1 *Joint interpretation of multi-/hyper-spectral images and LiDAR data*

Generally speaking, the process of joint interpretation is divided into three steps as shown in Figure 13: feature extraction to extract multi-level features, feature fusion to fuse the extracted heterogonous features effectively, and joint classification to discriminate landcovers accurately. The research on joint interpretation of multi-/hyper-spectral images and LiDAR data mainly focuses on feature fusion and joint classification.

The feature fusion methods of multi-/hyper-spectral images and LiDAR data can be summarized into four categories: feature stack methods, subspace-based methods, manifold learning-based methods and deep learning methods. Feature stack is the simplest and easiest way to implement feature fusion. This strategy forms an extended feature vector for each pixel in the remote sensing scene by stacking the height and intensity feature extracted from the LiDAR data after the spectral band of the multi-/hyper-spectral image [185]. In order to fully mine the discriminant information in multi-/hyper-spectral images and LiDAR data, morphological profiles (MPs) [186], attribute profiles (APs) [187] and extinction profiles (EPs) [188] are often used for multi-/hyper-spectral images and LiDAR data fusion because of their simple calculation efficiency, and can provide accurate classification results. However, stacking the

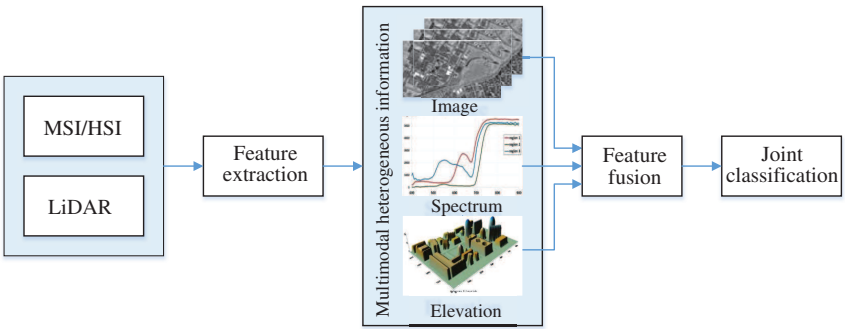

Figure 13 (Color online) General flowchart of joint interpretation of multi-/hyper-spectral images and LiDAR data.

spectral features, spatial features and elevation features extracted from the multi-/hyper-spectral and LiDAR data will increase the feature dimension of the samples, thus causing two major difficulties for subsequent classification tasks: dimension disaster and high computational complexity. The subspace-based methods can avoid the dimensionality disaster and improve the computational efficiency. Such methods also have the characteristics of improving the signal-to-noise ratio and the classification accuracy. Subspace-based methods assume that features extracted from multi-/hyper-spectral and LiDAR data can be represented in a low-dimensional subspace. In the original subspace model, both the basis of subspace and the characteristics after fusion are unknown and need to be estimated. In [189], orthogonal total variation component analysis (OTVCA) was introduced [40] into the subspace model to estimate the basis of subspace and the features after fusion simultaneously. Besides, based on the prior information of the spatial structure of remote sensing scene, constraint term was added to the subspace model to make the features after fusion smooth to the object expression. In [190], the authors took the two-dimensional wavelet basis as the basis of the subspace and used a sparse subspace model to model multi-/hyper-spectral images and LiDAR data fusion. Sparse and low-rank component analysis (SLCA) was used to solve the problem, and l_1 norm constrained wavelet coefficients were used to make the fused feature sparse in two-dimensional wavelet space. Manifold learning has also been used in multi-modal data fusion. Except for the aforementioned semi-supervised manifold alignment, in [191], the authors proposed a multi-feature learning framework, which can embed linear features and nonlinear features, combine the similarity measure information of samples in multi-feature space, and obtain the manifold distribution of samples in multi-feature space. Liao et al. proposed a series of multi-source sensor data fusion frameworks based on graph model. They adopted unsupervised [192], semi-supervised [193], supervised [194, 195] way to construct the graph model for each attribute feature extracted from multi-/hyper-spectral images and LiDAR data, and then, the fused graph is used to solve the manifold embedding mapping matrix to obtain the intrinsic characteristics of remote sensing scene in the low-dimensional space [192, 195]. At present, deep learning is developing rapidly in the field of remote sensing. Models of deep structure have the ability to extract high-order, multi-layer, abstract features from the input data, which are usually invariant to the nonlinear distribution of samples in the original space, and thus, deep learning methods are also applied to multi-/hyper-spectral images and LiDAR data fusion. Ghamisi et al. [188] fused the spatial, spectral and elevation features extracted from multi-/hyper-spectral images and LiDAR data by using the graph model, and input these fused features into a convolutional neural network (CNN) for higher-order feature extraction. In order to use the spatial and elevation information of multi-/hyper-spectral images and LiDAR data more effectively, Chen et al. designed a dual-channel deep learning model for the two data sources. In each channel, a CNN is used to extract features from a data source, and finally, a fully connected deep neural network is used to fuse and classify heterogeneous features output from the two channels [196]. On this basis, a three-channel deep learning model is designed for spatial, spectral and elevation features [197]. Zhang et al. [198] proposed a patch to patch convolutional neural network (PToP CNN), which takes HSIs and LiDAR data as input and extracts the spatial, spectral and elevation information of remote sensing scenes end-to-end.

As for joint classification of multi-/hyper-spectral images and LiDAR data, the flexible base kernel design and task-oriented model solving potential of MKL [199] have provided a complete set of theories for heterogeneous feature fusion. The spectral, spatial and elevation features extracted from HSIs and LiDAR data by local filtering, can be used together by composite kernel method, which can distinguish various features and fully mine the complementary information among them [200]. Li et al. [191] designed

a parameterless multi-feature learning method based on attribute morphological features and subspace multidimensional logistic regression, and applied the method to HSIs and LiDAR data multi-attribute feature learning. Aiming at the problem of high feature dimension and limited training samples in the joint classification of multi-/hyper-spectral images and LiDAR data, Zhang et al. [201] proposed an integrated multi-kernel active learning method. This approach can obtain more useful information for classification from unlabeled samples through active learning, and integrate the output probability of several multi-kernel classifiers by the principle of maximum divergence. Deep learning-based methods usually have a complete framework including feature extraction, fusion and classification, which have been described in the end of Subsection 4.3.1.

4.3.2 *HSE data processing*

Before retrieving spectral information about objects from LRI, the dimensionless and sensor specific LRI values must be radiometrically calibrated and range- and angle corrected. After that, the spectral information of each point cloud can be retrieved from LRI values. The information content of the new type data is vast and creates new prospects for various applications. (1) The HSE data enables a new class of spectral laser indices to be calculated as analogues to spectral indices derived from passive remote sensing data. Fueled by the increasing spectral availability, the biophysical and chemical surface properties can be mapped with HSE systems. This will promote the development of precision agriculture and the protection of cultural heritage. (2) HSE may also improve the separation of ground from vegetation returns and leaves from woody materials, which ultimately will improve the accuracy of LiDAR based land cover classification, automatic point cloud classification, and biomass estimates. (3) HSE may also improve the accuracy of terrain mapping. Fueled by the penetration characteristics of water at different wavelengths, the water depth estimate can be carried out by using HSE system, which can achieve the seamless terrain mapping coastal zone.

The related structure, location and measured spectrum show many prospects for agriculture and forestry applications of HSE. It could reliably and automatically detect many kinds of vegetation related to stress status, light-use efficiency of tree crowns [202,203], nitrogen contents estimation [204–206], biochemical parameters monitoring [207], chlorophyll level estimation [208, 209]. The HSE data with spectral and 3D spatial information simultaneously enhance the ability of target characterization and classification [210, 211]. According to the classification objects, the classification methods using multi-/hyper-spectral LiDAR data can be divided into two categories: image-based methods and point cloud-based methods. At present, most researches use image-based method to process multispectral LiDAR data. Firstly, the height image and intensity image of each band are generated by using multispectral point cloud data, and then traditional image processing methods can be used for classification. At present, Mahalanobis distance (MD) classifier [212], maximum likelihood classifier [213,214], SVM [215,216], random forest [212, 217] and decision tree classifier [218] are all used for rasterized multi-spectral LiDAR image classification. Some researchers directly classified the multi-spectral point clouds to realize the three-dimensional spatial classification of remote sensing scenes. In [219], the distribution information of the target in the three-dimensional space was extracted by PCA, and then was inputted into SVM with the multi-band intensity information for classification. Ekhtari et al. [220, 221] separated single echo point cloud from multiple echo point clouds when classifying multi-spectral point clouds. Compared with the image-based methods, the classification of point clouds can achieve higher classification accuracy [221–223].

In [224], in order to improve the ability of 3D land cover classification using multispectral point clouds, a geometric-spectral feature extraction model named tensor manifold discriminant embedding (TMDE) was proposed based on tensor representation. This model contains two parts. (1) Tensor representation of unorganized multispectral point clouds. Each point is represented as a second-order tensor, which is the information source for subsequent feature extraction. (2) Tensor-based feature extraction. Through keeping the intraclass samples' distribution and maximizing the distance between categories, the multilinear mapping matrices are obtained, which can project the second-order tensors into the feature space to extract the discriminative geometric-spectral features.

Given a training set $\mathcal{X} = \{\mathcal{X}_i\}, i = 1, 2, \ldots, N$ in high-dimensional space $\mathbb{R}^{I_1 \times I_2 \times \cdots \times I_M}$, the purpose is to search for N mapping matrices $\left\{\boldsymbol{U}_m \in \mathbb{R}^{P_m \times I_m}, P_m < I_m, m = 1, 2, \ldots, M\right\}$ that map $\mathcal{X}_i$ into $\mathcal{Y}_i \in \mathbb{R}^{P_1 \times P_2 \times \cdots \times P_M}, i = 1, 2, \ldots, N$. The intraclass neighborhood graph $\boldsymbol{G}_a$ and interclass neighborhood graph $\boldsymbol{G}_b$ are constructed firstly. Based on the maximum margin criterion (MMC) [225], the final objective

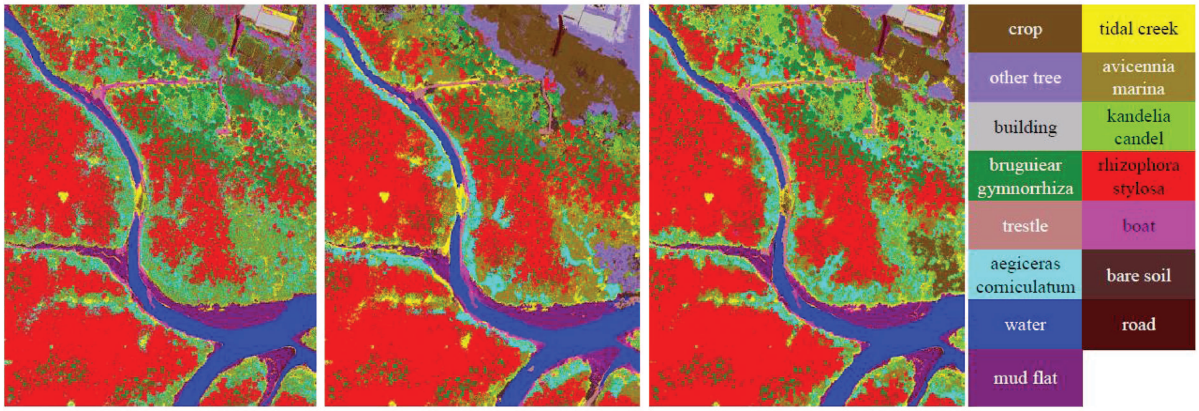

Figure 14 (Color online) Classification maps obtained by using (a) multispectral features, (b) multispectral features, DEM and DSM, and (c) multispectral features and *n*DSM.

function can be obtained as follows:

$$\underset{\mathcal{Y}_1,\mathcal{Y}_2,\ldots,\mathcal{Y}_N}{\arg\min} \left\{ \sum_{i,j}^{N} \boldsymbol{G}_a(i,j) \cdot \|\mathcal{Y}_i - \mathcal{Y}_j\|_F^2 - \sum_{i,j}^{N} \boldsymbol{G}_b(i,j) \cdot \|\mathcal{Y}_i - \mathcal{Y}_j\|_F^2 \right\}. \tag{2}$$

This problem can be solved by the eigenvalue decomposition, the solution $\boldsymbol{U}_m^* \in \mathbb{R}^{P_m \times I_m}$ is given by P_m eigenvectors associated with the least P_m eigenvalues. All the samples can be thus mapped into the low-dimensional features space by mode-k product as $\mathcal{Y}_i = \mathcal{X}_i \times_1 \boldsymbol{U}_1^* \times_2 \boldsymbol{U}_2^* \times \cdots \times_M \boldsymbol{U}_M^*$.

Based on the field test data of Shankou Mangrove National Ecology and Nature Reserve, we combined the 2D spatial, spectral and elevation (digital elevation model (DEM), digital surface model (DSM), normalized digital surface model (*n*DSM)) information to carry out the classification experiment, and the classification accuracies can reach more than 90%. Figure 14 shows the classification maps obtained by using different features. Figure 14(a) is obtained by using multispectral features. Figure 14(b) is obtained by using multispectral features, DEM and DSM. Figure 14(c) is obtained by using multispectral features and *n*DSM. The spectral difference between bruguiear gymnorrhiza and rhizophora stylosa was significant, and thus they can be well distinguished even only using multispectral features. However, for the avicennia marina and aegiceras corniculatum, their spectral characteristics are similar, and their growth is mixed and stratified. By combining the elevation information, the classification performance of these two kinds of mangroves has been improved.

4.4 Major issues in data processing

Expanding the use of LiDAR data to incorporate the spectral information has great potential to advance 4D $(x, y, z, R(\lambda))$ research and applications about HSI. On the road to realize this potential, ongoing researches have to confront the following two major issues.

(1) Accurate spectral reflectance retrieval of HSE. HSE intensity is affected by many factors, for example, incidence angle, an uncertain illumination condition, imaging range/distance. Radiometric calibration of HSE intensity is an important prerequisite for subsequent applications, such as land cover classification and object detection. Study in [202] illustrates the nonlinear relationship between target reflectance and reported HSE intensity. Therefore, retrieving the reflectivity information from HSE intensity values is the first step of research for HSE. Existing empirical radiometric calibration and relative models need to be improved, or new methods need to be presented to retrieve accurate spectral reflectance of the target.

(2) Analysis and display of HSE. Data volumes of HSE datasets are large, and will increase with the expansion of the spectral dimension. Hence, there is a need to develop the management and analysis approaches for the new HSE data. Existing softwares can only display 3D information (x, y, z) or $(x, y, R(\lambda))$ at the same time. How to display the 4D information $(x, y, z, R(\lambda))$ provided by HSE will become an important content.

5 Conclusion

Recently, hyperspectral remote sensing presents new trends and is progressively developing from traditional two-dimensional detection to multi-dimensional, real-time and stereoscopic remote sensing. In this paper, the current researches on hyperspectral remote sensing and image processing have been reviewed. After that, three typical modes of advanced hyperspectral remote sensing have been introduced in details, including MultiTemp-HSI with multitemporal hyperspectral imaging, HSV with real-time spectral imaging and HSE with 3D spectral imaging. The introduction to the multimodal HSI covers the fundamental principle, data acquisition, processing and applications, and major issues in data processing for each mode.

The multimodal HSI remote sensing is really emerging. To meet the potential challenges, involving highly complex nonlinearity, heterogeneity and sparsity in data processing, and lack of benchmark dataset for scientific research, on the one hand, researchers should develop new theories and methods for multimodal and multidimensional signal processing; on the other hand, it is also important to extend the existing theories and methods in conventional hyperspectral remote sensing by combining with new data processing techniques to solve the new challenges raised by the multimodal HSI. High-order tensor representation has a good potential for the data representation of complex multimodal HSI, since 3-order tensor has successfully applied in HSI interpretation [226, 227]. Deep learning can be used to help with establishing framework of feature learning, however, there are relatively few emerging multimodal hyperspectral data, and thus how to make the model overcome the dependence on a large number of training samples needs further study. Furthermore, with aid of the multimodal hyperspectral remote sensing and new applicative processing approaches, new ways of object interpretation, such as 3D change detection, real-time object tracking and dynamic scene understanding will be attractive and achievable.

Acknowledgements This work was supported by National Natural Science Foundation of Key International Cooperation of China (Grant No. 61720106002) and National Key R&D Program of China (Grant No. 2017YFC1405100). The authors would like to thank Beijing Anzhou Technology Co. LTD for providing the HSV data shown in Figure 7.

References

1 Green R O, Chrien T G, Enmark H T. First results from the airborne visible/infrared imaging spectrometer (AVIRIS). Remote Sens Environ, 1987, 44: 127–143
2 Sankey T T, McVay J, Swetnam T L, et al. UAV hyperspectral and lidar data and their fusion for arid and semi-arid land vegetation monitoring. Remote Sens Ecol Conserv, 2018, 4: 20–33
3 Govender M, Chetty K, Bulcock H. A review of hyperspectral remote sensing and its application in vegetation and water resource studies. Water Sa, 2007, 33: 145–152
4 Luo B, Yang C, Chanussot J, et al. Crop yield estimation based on unsupervised linear unmixing of multidate hyperspectral imagery. IEEE Trans Geosci Remote Sens, 2012, 51: 162–173
5 Morier T, Cambouris A N, Chokmani K. In-season nitrogen status assessment and yield estimation using hyperspectral vegetation indices in a potato crop. Agronomy J, 2015, 107: 1295–1309
6 Moroni M, Lupo E, Marra E, et al. Hyperspectral image analysis in environmental monitoring: setup of a new tunable filter platform. Procedia Environ Sci, 2013, 19: 885–894
7 Honkavaara E, Hakala T, Markelin L, et al. Autonomous hyperspectral UAS photogrammetry for environmental monitoring applications. ISPRS Archives, 2014, XL-1: 155–159
8 Luft L, Neumann C, Freude M, et al. Hyperspectral modeling of ecological indicators — a new approach for monitoring former military training areas. Ecol Indicators, 2014, 46: 264–285
9 Mucher C A, Kooistra L, Vermeulen M, et al. Quantifying structure of Natura 2000 heathland habitats using spectral mixture analysis and segmentation techniques on hyperspectral imagery. Ecol Indic, 2013, 33: 71–81
10 Briottet X, Boucher Y, Dimmeler A, et al. Military applications of hyperspectral imagery. In: Proceedings of SPIE, Defense and Security Symposium, Orlando, 2006. 6239: 62390B
11 Kastek M, Piatkowski T, Dulski R, et al. Multispectral and hyperspectral measurements of soldier's camouflage equipment. In: Proceedings of SPIE, Defense, Security, and Sensing, Baltimore, 2012. 8382: 83820K
12 Richards J A, Jia X. Remote Sensing Digital Image Analysis. Berlin: Springer, 1999
13 Tong Q, Xue Y, Zhang L. Progress in hyperspectral remote sensing science and technology in china over the past three decades. IEEE J Sel Top Appl Earth Observ Remote Sens, 2014, 7: 70–91
14 Gerhart T, Sunu J, Lieu L, et al. Detection and tracking of gas plumes in LWIR hyperspectral video sequence data. In: Proceedings of SPIE, Defense, Security, and Sensing, Baltimore, 2013. 8743: 87430J
15 Tochon G, Chanussot J, Gilles J, et al. Gas plume detection and tracking in hyperspectral video sequences using binary partition trees. In: Proceedings of IEEE Workshop on Hyperspectral Image and Signal Processing: Evolution in Remote Sensing (WHISPERS), Lausanne, 2014. 1–4
16 Shaw G, Manolakis D. Signal processing for hyperspectral image exploitation. IEEE Signal Process Mag, 2002, 19: 12–16
17 Stein D W J, Beaven S G, Hoff L E, et al. Anomaly detection from hyperspectral imagery. IEEE Signal Process Mag, 2002, 19: 58–69
18 Manolakis D, Shaw G. Detection algorithms for hyperspectral imaging applications. IEEE Signal Process Mag, 2002, 19: 29–43
19 Keshava N, Mustard J F. Spectral unmixing. IEEE Signal Process Mag, 2002, 19: 44–57
20 Landgrebe D. Hyperspectral image data analysis. IEEE Signal Process Mag, 2002, 19: 17–28

21 Camps-Valls G, Tuia D, Bruzzone L, et al. Advances in hyperspectral image classification. IEEE Signal Process Mag, 2014, 31: 45–54
22 Manolakis D, Truslow E, Pieper M, et al. Detection algorithms in hyperspectral imaging systems: an overview of practical algorithms. IEEE Signal Process Mag, 2014, 31: 24–33
23 Nasrabadi N M. Hyperspectral target detection: an overview of current and future challenges. IEEE Signal Process Mag, 2014, 31: 34–44
24 Li W, Du Q. A survey on representation-based classification and detection in hyperspectral remote sensing imagery. Pattern Recognit Lett, 2015, 83: 115–123
25 Arce G R, Brady D J, Carin L, et al. Compressive coded aperture spectral imaging: an introduction. IEEE Signal Process Mag, 2014, 31: 105–115
26 Willett R, Duarte M, Davenport M, et al. Sparsity and structure in hyperspectral imaging: sensing, reconstruction, and target detection. IEEE Signal Process Mag, 2014, 31: 116–126
27 Sami ul H Q, Tao L M, Sun F C, et al. A fast and robust sparse approach for hyperspectral data classification using a few labeled samples. IEEE Trans Geosci Remote Sens, 2012, 50: 2287–2302
28 Chen Y, Nasrabadi N M, Tran T D. Sparse representation for target detection in hyperspectral imagery. IEEE J Sel Top Appl Earth Observ Remote Sens, 2011, 5: 629–640
29 Chen J, Jiao L. Hyperspectral imagery classification using local collaborative representation. Int J Remote Sens, 2015, 36: 734–748
30 Li W, Du Q. Collaborative representation for hyperspectral anomaly detection. IEEE Trans Geosci Remote Sens, 2015, 53: 1463–1474
31 Zhang H, Li J, Huang Y, et al. A nonlocal weighted joint sparse representation classification method for hyperspectral imagery. IEEE J Sel Top Appl Earth Observ Remote Sens, 2014, 7: 2056–2065
32 Li J, Zhang H, Zhang L, et al. Hyperspectral anomaly detection by the use of background joint sparse representation. IEEE J Sel Top Appl Earth Observ Remote Sens, 2015, 8: 2523–2533
33 Chen Y, Nasrabadi N M, Tran T D. Simultaneous joint sparsity model for target detection in hyperspectral imagery. IEEE Geosci Remote Sens Lett, 2011, 8: 676–680
34 Li W, Du Q. Joint within-class collaborative representation for hyperspectral image classification. IEEE J Sel Top Appl Earth Observ Remote Sens, 2014, 7: 2200–2208
35 Li J, Zhang H, Huang Y, et al. Hyperspectral image classification by nonlocal joint collaborative representation with a locally adaptive dictionary. IEEE Trans Geosci Remote Sens, 2014, 52: 3707–3719
36 Chen Y, Nasrabadi N M, Tran T D. Hyperspectral image classification via kernel sparse representation. IEEE Trans Geosci Remote Sens, 2013, 51: 217–231
37 Liu J, Wu Z, Wei Z, et al. Spatial-spectral kernel sparse representation for hyperspectral image classification. IEEE J Sel Top Appl Earth Observ Remote Sens, 2013, 6: 2462–2471
38 Li W, Du Q, Xiong M. Kernel collaborative representation with Tikhonov regularization for hyperspectral image classification. IEEE Geosci Remote Sens Lett, 2015, 12: 48–52
39 Li J Y, Zhang H Y, Zhang L P. Column-generation kernel nonlocal joint collaborative representation for hyperspectral image classification. ISPRS J Photogrammetry Remote Sens, 2014, 94: 25–36
40 Camps-Valls G, Bruzzone L. Kernel-based methods for hyperspectral image classification. IEEE Trans Geosci Remote Sens, 2005, 43: 1351–1362
41 Mountrakis G, Im J, Ogole C. Support vector machines in remote sensing: a review. ISPRS J Photogrammetry Remote Sens, 2011, 66: 247–259
42 Niazmardi S, Demir B, Bruzzone L, et al. Multiple kernel learning for remote sensing image classification. IEEE Trans Geosci Remote Sens, 2018, 56: 1425–1443
43 Gu Y, Chanussot J, Jia X, et al. Multiple kernel learning for hyperspectral image classification: a review. IEEE Trans Geosci Remote Sens, 2017, 55: 6547–6565
44 Gu Y, Wang C, You D, et al. Representative multiple kernel learning for classification in hyperspectral imagery. IEEE Trans Geosci Remote Sens, 2012, 50: 2852–2865
45 Gu Y F, Wang Q W, Jia X P, et al. A novel MKL model of integrating LiDAR data and MSI for urban area classification. IEEE Trans Geosci Remote Sens, 2015, 53: 5312–5326
46 Gu Y, Wang Q, Wang H, et al. Multiple kernel learning via low-rank nonnegative matrix factorization for classification of hyperspectral imagery. IEEE J Sel Top Appl Earth Observ Remote Sens, 2014, 8: 2739–2751
47 Wang Q, Gu Y, Tuia D. Discriminative multiple kernel learning for hyperspectral image classification. IEEE Trans Geosci Remote Sens, 2016, 54: 3912–3927
48 Liu T, Gu Y, Jia X, et al. Class-specific sparse multiple kernel learning for spectral-spatial hyperspectral image classification. IEEE Trans Geosci Remote Sens, 2016, 54: 7351–7365
49 Rakotomamonjy A, Bach F, Stephane C, et al. SimpleMKL. J Mach Learn Res, 2008, 9: 2491–2521
50 Gu Y, Gao G, Zuo D, et al. Model selection and classification with multiple kernel learning for hyperspectral images via sparsity. IEEE J Sel Top Appl Earth Observ Remote Sens, 2014, 7: 2119–2130
51 Gu Y, Wang Q, Xie B. Multiple kernel sparse representation for airborne LiDAR data classification. IEEE Trans Geosci Remote Sens, 2016, 55: 1085–1105
52 Gu Y, Liu H. Sample-screening MKL method via boosting strategy for hyperspectral image classification. Neurocomputing, 2015, 173: 1630–1639
53 Wang Y, Gu Y, Gao G, et al. Hyperspectral image classification with multiple kernel Boosting algorithm. In: Proceedings of IEEE International Conference on Image Processing, Paris, 2015. 5047–5051
54 Gu Y, Liu T, Jia X, et al. Nonlinear multiple kernel learning with multiple-structure-element extended morphological profiles for hyperspectral image classification. IEEE Trans Geosci Remote Sens, 2016, 54: 3235–3247
55 Lunga D, Prasad S, Crawford M M, et al. Manifold-learning-based feature extraction for classification of hyperspectral data: a review of advances in manifold learning. IEEE Signal Process Mag, 2014, 31: 55–66
56 Hong D, Yokoya N, Zhu X X. Learning a robust local manifold representation for hyperspectral dimensionality reduction. IEEE J Sel Top Appl Earth Observ Remote Sens, 2017, 10: 2960–2975
57 He J, Zhang L, Wang Q, et al. Using diffusion geometric coordinates for hyperspectral imagery representation. IEEE Geosci Remote Sens Lett, 2009, 6: 767–771
58 Mohan A, Sapiro G, Bosch E. Spatially coherent nonlinear dimensionality reduction and segmentation of hyperspectral

images. IEEE Geosci Remote Sens Lett, 2007, 4: 206–210
59 Ma L, Zhang X, Yu X, et al. Spatial regularized local manifold learning for classification of hyperspectral images. IEEE J Sel Top Appl Earth Observ Remote Sens, 2015, 9: 609–624
60 Ma L, Crawford M M, Yang X, et al. Local-manifold-learning-based graph construction for semisupervised hyperspectral image classification. IEEE Trans Geosci Remote Sensing, 2014, 53: 2832–2844
61 Ziemann A K, Messinger D W. An adaptive locally linear embedding manifold learning approach for hyperspectral target detection. In: Proceedings of SPIE Defense and Security, Baltimore, 2015. 9472: 94720O
62 Ziemann A K, Theiler J, Messinger D W. Hyperspectral target detection using manifold learning and multiple target spectra. In: Proceedings of IEEE Applied Imagery Pattern Recognition Workshop (AIPR), Washington, 2015. 1–7
63 Heylen R, Scheunders P. Calculation of geodesic distances in nonlinear mixing models: application to the generalized bilinear model. IEEE Geosci Remote Sens Lett, 2012, 9: 644–648
64 Chi J, Crawford M M. Selection of landmark points on nonlinear manifolds for spectral unmixing using local homogeneity. Geosci Remote Sens Lett IEEE, 2012, 10: 711–715
65 Chen Y, Lin Z, Zhao X, et al. Deep learning-based classification of hyperspectral data. IEEE J Sel Top Appl Earth Observ Remote Sens, 2014, 7: 2094–2107
66 Gao L, Gu D, Zhuang L, et al. Combining t-distributed stochastic neighbor embedding with convolutional neural networks for hyperspectral image classification. IEEE Geosci Remote Sens Lett, 2020, 17: 1368–1372
67 Zhang L, Zhang L, Du B. Deep learning for remote sensing data: a technical tutorial on the state of the art. IEEE Geosci Remote Sens Mag, 2016, 4: 22–40
68 Audebert N, Le Saux B, Lefevre S. Deep learning for classification of hyperspectral data: a comparative review. IEEE Geosci Remote Sens Mag, 2019, 7: 159–173
69 Rasti B, Hong D, Hang R, et al. Feature extraction for hyperspectral imagery: the evolution from shallow to deep. IEEE Geosci Remote Sens Mag, 2020. doi: 10.1109/MGRS.2020.2979764
70 Ghamisi P, Maggiori E, Li S T, et al. New frontiers in spectral-spatial hyperspectral image classification: the latest advances based on mathematical morphology, markov random fields, segmentation, sparse representation, and deep learning. IEEE Geosci Remote Sens Mag, 2018, 6: 10–43
71 Xu F, Hu C, Li J, et al. Special focus on deep learning in remote sensing image processing. Sci China Inf Sci, 2020, 63: 140300
72 Li J, Li Y F, He L, et al. Spatio-temporal fusion for remote sensing data: an overview and new benchmark. Sci China Inf Sci, 2020, 63: 140301
73 Li Y F, Li J, He L, et al. A new sensor bias-driven spatio-temporal fusion model based on convolutional neural networks. Sci China Inf Sci, 2020, 63: 140302
74 Hou X Y, Ao W, Song Q, et al. FUSAR-Ship: building a high-resolution SAR-AIS matchup dataset of Gaofen-3 for ship detection and recognition. Sci China Inf Sci, 2020, 63: 140303
75 Cui K, Hu C, Wang R, et al. Deep-learning-based extraction of the animal migration patterns from weather radar images. Sci China Inf Sci, 2020, 63: 140304
76 He N J, Fang L Y, Plaza A. Hybrid first and second order attention Unet for building segmentation in remote sensing images. Sci China Inf Sci, 2020, 63: 140305
77 Liu X B, Qiao Y L, Xiong Y H, et al. Cascade conditional generative adversarial nets for spatial-spectral hyperspectral sample generation. Sci China Inf Sci, 2020, 63: 140306
78 Gu Y F, Liu H, Wang T F, et al. Deep feature extraction and motion representation for satellite video scene classification. Sci China Inf Sci, 2020, 63: 140307
79 Lahat D, Adali T, Jutten C. Multimodal data fusion: an overview of methods, challenges, and prospects. Proc IEEE, 2015, 103: 1449–1477
80 Dalla M M, Prasad S, Pacifici F, et al. Challenges and opportunities of multimodality and data fusion in remote sensing. Proc IEEE, 2015, 103: 1585–1601
81 Gomez-Chova L, Tuia D, Moser G, et al. Multimodal classification of remote sensing images: a review and future directions. Proc IEEE, 2015, 103: 1560–1584
82 Camps-Valls G, Gomez-Chova L, Munoz-Mari J, et al. Composite kernels for hyperspectral image classification. IEEE Geosci Remote Sens Lett, 2006, 3: 93–97
83 Tuia D, Ratle F, Pozdnoukhov A, et al. Multisource composite kernels for urban-image classification. IEEE Geosci Remote Sens Lett, 2010, 7: 88–92
84 Volpi M, Camps-Valls G, Tuia D. Spectral alignment of multi-temporal cross-sensor images with automated kernel canonical correlation analysis. ISPRS J Photogrammetry Remote Sens, 2015, 107: 50–63
85 Tuia D, Camps-Valls G, Matasci G, et al. Learning relevant image features with multiple-kernel classification. IEEE Trans Geosci Remote Sens, 2010, 48: 3780–3791
86 Liu W, Qin R. A multikernel domain adaptation method for unsupervised transfer learning on cross-source and cross-region remote sensing data classification. IEEE Trans Geosci Remote Sens, 2020, 58: 4279–4289
87 Li S, Yin H, Fang L. Remote sensing image fusion via sparse representations over learned dictionaries. IEEE Trans Geosci Remote Sens, 2013, 51: 4779–4789
88 Cheng M, Wang C, Li J. Sparse representation based pansharpening using trained dictionary. IEEE Geosci Remote Sens Lett, 2014, 11: 293–297
89 Ghahremani M, Ghassemian H. Remote sensing image fusion using ripplet transform and compressed sensing. IEEE Geosci Remote Sens Lett, 2015, 12: 502–506
90 Zhao C, Gao X, Emery W J, et al. An integrated spatio-spectral-temporal sparse representation method for fusing remote-sensing images with different resolutions. IEEE Trans Geosci Remote Sens, 2018, 56: 1–13
91 Vargas E, Arguello H, Tourneret J Y. Spectral image fusion from compressive measurements using spectral unmixing and a sparse representation of abundance maps. IEEE Trans Geosci Remote Sens, 2019, 57: 5043–5053
92 Romero A, Gatta C, Camps-Valls G. Unsupervised deep feature extraction for remote sensing image classification. IEEE Trans Geosci Remote Sens, 2015, 54: 1–14
93 Tuia D, Flamary R, Courty N. Multiclass feature learning for hyperspectral image classification: sparse and hierarchical solutions. ISPRS J Photogrammetry Remote Sens, 2015, 105: 272–285
94 Zhang H, Ni W, Yan W, et al. Registration of multimodal remote sensing image based on deep fully convolutional neural network. IEEE J Sel Top Appl Earth Observ Remote Sens, 2019, 12: 3028–3042

95 Benedetti P, Ienco D, Gaetano R, et al. M^3Fusion: a deep learning architecture for multiscale multimodal multitemporal satellite data fusion. IEEE J Sel Top Appl Earth Observ Remote Sens, 2018, 11: 4939–4949
96 Tuia D, Volpi M, Trolliet M, et al. Semisupervised manifold alignment of multimodal remote sensing images. IEEE Trans Geosci Remote Sens, 2014, 52: 7708–7720
97 Matasci G, Volpi M, Kanevski M, et al. Semisupervised transfer component analysis for domain adaptation in remote sensing image classification. IEEE Trans Geosci Remote Sens, 2015, 53: 3550–3564
98 Chi M, Sun Z, Qin Y, et al. A novel methodology to label urban remote sensing images based on location-based social media photos. Proc IEEE, 2017, 105: 1926–1936
99 Li J, Benediktsson J A, Zhang B, et al. Spatial technology and social media in remote sensing: a survey. Proc IEEE, 2017, 105: 1855–1864
100 Wang H, Skau E, Krim H, et al. Fusing heterogeneous data: a case for remote sensing and social media. IEEE Trans Geosci Remote Sens, 2018, 56: 6956–6968
101 Qi L, Li J, Wang Y, et al. Urban observation: integration of remote sensing and social media data. IEEE J Sel Top Appl Earth Observ Remote Sens, 2019, 12: 4252–4264
102 Singh A. Digital change detection techniques using remotely-sensed data. Int J Remote Sens, 1989, 10: 989–1003
103 Heo J, Fitzhugh T W. A standardized radiometric normalization method for change detection using remotely sensed imagery. Photogramm Eng Remote Sens, 2000, 66: 173–181
104 Schowengerdt R A. Remote Sensing: Models and Methods for Image Processing. 2nd ed. New York: Academic, 1997
105 Gonzalez R, Woods R. Digital Image Processing. 2nd ed. Englewood Cliffs: Prentice-Hall, 2002
106 Inamdar S, Bovolo F, Bruzzone L, et al. Multidimensional probability density function matching for preprocessing of multitemporal remote sensing images. IEEE Trans Geosci Remote Sens, 2008, 46: 1243–1252
107 Gorretta N, Hadoux X, Jay S. Multi-temporal hyperspectral data classification without explicit reflectance correction. In: Proceedings of IEEE International Geoscience and Remote Sensing Symposium (IGARSS), Milan, 2015. 4228–4231
108 Hemissi S, Farah I R, Ettabaa K S, et al. A robust evidential fisher discriminant for multi-temporal hyperspectral images classification. In: Proceedings of IEEE International Geoscience and Remote Sensing Symposium (IGARSS), Munich, 2012. 4275–4278
109 Jin H, Li P, Fan W. Land cover classification using multitemporal CHRIS/PROBA images and multitemporal texture. In: Proceedings of IEEE International Geoscience and Remote Sensing Symposium (IGARSS), Boston, 2008. 742–745
110 Prasad S, Bruce L M, Kalluri H. A robust multi-classifier decision fusion framework for hyperspectral, multi-temporal classification. In: Proceedings of IEEE International Geoscience and Remote Sensing Symposium (IGARSS), Boston, 2008, 273–276
111 Tuia D, Persello C, Bruzzone L. Domain adaptation for the classification of remote sensing data: an overview of recent advances. IEEE Geosci Remote Sens Mag, 2016, 4: 41–57
112 Ye M, Qian Y, Zhou J, et al. Dictionary learning-based feature-level domain adaptation for cross-scene hyperspectral image classification. IEEE Trans Geosci Remote Sens, 2017, 55: 1544–1562
113 Kim W, Crawford M M. Adaptive classification for hyperspectral image data using manifold regularization kernel machines. IEEE Trans Geosci Remote Sens, 2010, 48: 4110–4121
114 Yang H L, Crawford M M. Spectral and spatial proximity-based manifold alignment for multitemporal hyperspectral image classification. IEEE Trans Geosci Remote Sens, 2016, 54: 51–64
115 Yang H L, Crawford M M. Domain adaptation with preservation of manifold geometry for hyperspectral image classification. IEEE J Sel Top Appl Earth Observ Remote Sens, 2016, 9: 543–555
116 Nielsen A A, Canty M J. Kernel principal component and maximum autocorrelation factor analyses for change detection. In: Proceedings of SPIE, Remote Sensing, Berlin, 2009. 7477: 74770T
117 Nielsen A A. The regularized iteratively reweighted MAD method for change detection in multi- and hyperspectral data. IEEE Trans Image Process, 2007, 16: 463–478
118 Xia J, Yokoya N, Iwasaki A. Ensemble of transfer component analysis for domain adaptation in hyperspectral remote sensing image classification. In: Proceedings of IEEE International Geoscience and Remote Sensing Symposium (IGARSS), Fort Worth, 2017. 4762–4765
119 Samat A, Gamba P, Abuduwaili J, et al. Geodesic flow kernel support vector machine for hyperspectral image classification by unsupervised subspace feature transfer. Remote Sens, 2016, 8: 234
120 Gao G, Gu Y. Tensorized principal component alignment: a unified framework for multimodal high-resolution images classification. IEEE Trans Geosci Remote Sens, 2018, 57: 46–61
121 Li T, Gu Y. Joint tensor subspace alignment on multi-angular remote sensing image. In: Proceedings of IEEE Workshop on Hyperspectral Image and Signal Processing: Evolution in Remote Sensing (WHISPERS), Amsterdam, 2018. 1–5
122 Qin Y, Bruzzone L, Li B. Tensor alignment based domain adaptation for hyperspectral image classification. IEEE Trans Geosci Remote Sens, 2019, 57: 9290–9307
123 Persello C, Bruzzone L. Active learning for domain adaptation in the supervised classification of remote sensing images. IEEE Trans Geosci Remote Sens, 2012, 50: 4468–4483
124 Banerjee B, Bovolo F, Bhattacharya A, et al. A novel graph-matching-based approach for domain adaptation in classification of remote sensing image pair. IEEE Trans Geosci Remote Sens, 2015, 53: 4045–4062
125 Tuia D, Munoz-Mari J, Gomez-Chova L, et al. Graph matching for adaptation in remote sensing. IEEE Trans Geosci Remote Sens, 2013, 51: 329–341
126 Jacobs J P, Thoonen G, Tuia D, et al. Domain adaptation with hidden Markov random fields. In: Proceedings of IEEE International Geoscience and Remote Sensing Symposium (IGARSS), Melbourne, 2013. 3112–3115
127 Ettabaa K S, Hamdi M A, Salem R B. SVM for hyperspectral images classification based on 3D spectral signature. In: Proceedings of International Conference on Advanced Technologies for Signal and Image Processing (ATSIP), Sousse, 2014. 42–47
128 Hemissi S, Farah I R, Ettabaa K S, et al. Multi-spectro-temporal analysis of hyperspectral imagery based on 3-D spectral modeling and multilinear algebra. IEEE Trans Geosci Remote Sens, 2012, 51: 199–216
129 Teke M, Yardimci Y. Classification of crops using multitemporal hyperion images. In: Proceedings of IEEE International Conference on Agro-Geoinformatics, Istanbul, 2015. 282–287
130 Othman E, Bazi Y, Alajlan N, et al. Three-layer convex network for domain adaptation in multitemporal VHR images. IEEE Geosci Remote Sens Lett, 2016, 13: 354–358
131 Elshamli A, Taylor G W, Berg A, et al. Domain adaptation using representation learning for the classification of remote

sensing images. IEEE J Sel Top Appl Earth Observ Remote Sens, 2017, 99: 1–12
132 Yang J, Zhao Y Q, Chan J C W. Learning and transferring deep joint spectral-spatial features for hyperspectral classification. IEEE Trans Geosci Remote Sens, 2017, 55: 4729–4742
133 Hong D, Yokoya N, Ge N, et al. Learnable manifold alignment (LeMA): a semi-supervised cross-modality learning framework for land cover and land use classification. ISPRS J Photogrammetry Remote Sens, 2019, 147: 193–205
134 Tuia D, Campsvalls G. Kernel manifold alignment for domain adaptation. Plos One, 2016, 11: e0148655
135 Li X, Zhang L, Du B, et al. On gleaning knowledge from cross domains by sparse subspace correlation analysis for hyperspectral image classification. IEEE Trans Geosci Remote Sens, 2019, 57: 3204–3220
136 Qin Y, Bruzzone L, Li B, et al. Cross-domain collaborative learning via cluster canonical correlation analysis and random walker for hyperspectral image classification. IEEE Trans Geosci Remote Sens, 2019, 57: 3952–3966
137 Hong D, Yokoya N, Chanussot J, et al. Cospace: common subspace learning from hyperspectral-multispectral correspondences. IEEE Trans Geosci Remote Sens, 2019, 57: 4349–4359
138 Liu T, Zhang X, Gu Y. Unsupervised cross-temporal classification of hyperspectral images with multiple geodesic flow kernel learning. IEEE Trans Geosci Remote Sens, 2019, 57: 9688–9701
139 Gong B, Shi Y, Sha F, et al. Geodesic flow kernel for unsupervised domain adaptation. In: Proceedings of 2012 IEEE Conference on Computer Vision and Pattern Recognition, Providence, 2012. 2066–2073
140 Liu S, Bruzzone L, Bovolo F, et al. Sequential spectral change vector analysis for iteratively discovering and detecting multiple changes in hyperspectral images. IEEE Trans Geosci Remote Sens, 2015, 53: 4363–4378
141 Liu S, Bruzzone L, Bovolo F, et al. Unsupervised multitemporal spectral unmixing for detecting multiple changes in hyperspectral images. IEEE Trans Geosci Remote Sens, 2016, 54: 2733–2748
142 Cesmeci D, Karaca A C, Erturk A, et al. Hyperspectral change detection by multi-band census transform. In: Proceedings of IEEE Geoscience and Remote Sensing Symposium (IGARSS), Quebec, 2014. 2969–2972
143 Wu C, Zhang L, Du B. Hyperspectral anomaly change detection with slow feature analysis. Neurocomputing, 2015, 151: 175–187
144 Du B, Ru L, Wu C, et al. Unsupervised deep slow feature analysis for change detection in multi-temporal remote sensing images. IEEE Trans Geosci Remote Sens, 2019, 57: 9976–9992
145 Yuan Y, Lv H, Lu X. Semi-supervised change detection method for multi-temporal hyperspectral images. Neurocomputing, 2015, 148: 363–375
146 Wu C, Zhang L, Du B. Targeted change detection for stacked multi-temporal hyperspectral image. In: Proceedings of IEEE Workshop on Hyperspectral Image and Signal Processing: Evolution in Remote Sensing (WHISPERS), Shanghai, 2012. 1–4
147 Hazel G G. Object-level change detection in spectral imagery. IEEE Trans Geosci Remote Sens, 2001, 39: 553–561
148 Messinger D W, Richardson M, Casey J. Analysis of a multitemporal hyperspectral dataset over a common target scene. In: Proceedings of SPIE, Defense and Security Symposium, Orlando, 2006. 6233: 62331I
149 Sun Y, Zhang X, Shuai T, et al. Radiometric normalization of multitemporal hyperspectral satellite images. In: Proceedings of IEEE Geoscience and Remote Sensing Symposium (IGARSS), Quebec, 2014. 4204–4207
150 Halimi A, Dobigeon N, Toumeret J Y, et al. Unmixing multitemporal hyperspectral images accounting for endmember variability. In: Proceedings of IEEE European Signal Processing Conference (EUSIPCO), Nice, 2015. 1656–1660
151 Thouvenin P A, Dobigeon N, Tourneret J Y. A hierarchical Bayesian model accounting for endmember variability and abrupt spectral changes to unmix multitemporal hyperspectral images. IEEE Trans Comput Imaging, 2017, 4: 32–45
152 Thouvenin P A, Dobigeon N, Tourneret J Y. Unmixing multitemporal hyperspectral images with variability: an online algorithm. In: Proceedings of IEEE International Conference on Acoustics, Speech and Signal Processing (ICASSP), Shanghai, 2016. 3351–3355
153 Thouvenin P A, Dobigeon N, Tourneret J Y. Online unmixing of multitemporal hyperspectral images accounting for spectral variability. IEEE Trans Image Process, 2016, 25: 3979–3990
154 Henrot S, Chanussot J, Jutten C. Dynamical spectral unmixing of multitemporal hyperspectral images. IEEE Trans Image Process, 2016, 25: 3219–3232
155 Licciardi G A, Frate F D. Pixel unmixing in hyperspectral data by means of neural networks. IEEE Trans Geosci Remote Sens, 2011, 49: 4163–4172
156 Erturk A, Plaza A. Informative change detection by unmixing for hyperspectral images. IEEE Geosci Remote Sens Lett, 2015, 12: 1252–1256
157 Liu S, Bruzzone L, Bovolo F, et al. Multitemporal spectral unmixing for change detection in hyperspectral images. In: Proceedings of IEEE International Geoscience and Remote Sensing Symposium (IGARSS), Milan, 2015. 4165–4168
158 Erturk A, Iordache M D, Plaza A. Sparse unmixing-based change detection for multitemporal hyperspectral images. IEEE J Sel Top Appl Earth Observ Remote Sens, 2015, 9: 708–719
159 Erturk A, Iordache M D, Plaza A. Sparse unmixing with dictionary pruning for hyperspectral change detection. IEEE J Sel Top Appl Earth Observ Remote Sens, 2016, 10: 321–330
160 Torres-Madronero M C, Velez-Reyes M, van Bloem S J, et al. Multi-temporal unmixing analysis of Hyperion images over the Guanica Dry Forest. In: Proceedings of IEEE Workshop on Hyperspectral Image and Signal Processing: Evolution in Remote Sensing (WHISPERS), Lisbon, 2011. 1–4
161 Cerra D, Muller R, Reinartz P. Cloud removal in image time series through unmixing. In: Proceedings of International Workshop on the Analysis of Multitemporal Remote Sensing Images, Annecy, 2015. 1–4
162 Dombrowski M, Bajaj J, Willson P. Video-rate visible to LWIR hyperspectral imaging and image exploitation. In: Proceedings of IEEE Applied Imagery Pattern Recognition Workshop, Washington, 2002. 178–185
163 Arnold T, de Biasio M, Leitner R. Hyperspectral video endoscope for intra-surgery tissue classification using auto-fluorescence and reflectance spectroscopy. In: Proceedings of SPIE, European Conference on Biomedical Optics, Munich, 2011. 8087: 808711
164 Banerjee A, Burlina P, Broadwater J. Hyperspectral video for illumination-invariant tracking. In: Proceedings of IEEE Workshop on Hyperspectral Image and Signal Processing: Evolution in Remote Sensing (WHISPERS), Grenoble, 2009. 1–4
165 van Nguyen H, Banerjee A, Chellappa R. Tracking via object reflectance using a hyperspectral video camera. In: Proceedings of IEEE Computer Society Conference on Computer Vision and Pattern Recognition-Workshops, San Francisco, 2010. 44–51
166 Bodkin A, Sheinis A, Norton A, et al. Video-rate chemical identification and visualization with snapshot hyperspectral imaging. In: Proceedings of SPIE Defense, Security, and Sensing, Baltimore, 2012. 8374: 83740C
167 Merkurjev E, Sunu J, Bertozzi A L. Graph MBO method for multiclass segmentation of hyperspectral stand-off detection video. In: Proceedings of IEEE International Conference on Image Processing (ICIP), Paris, 2014. 689–693

168 Hu H, Sunu J, Bertozzi A L. Multi-class graph Mumford-Shah model for plume detection using the MBO scheme. In: Proceedings of International Workshop on Energy Minimization Methods in Computer Vision and Pattern Recognition, Hongkong, 2015. 209–222
169 Tochon G, Pauwels D, Dalla M M, et al. Unmixing-based gas plume tracking in LWIR hyperspectral video sequences. In: Proceedings of IEEE Workshop on Hyperspectral Image and Signal Processing: Evolution in Remote Sensing (WHISPERS), Los Angeles, 2016. 1–5
170 Xu Y, Wu Z, Wei Z, et al. GAS plume detection in hyperspectral video sequence using low rank representation. In: Proceedings of IEEE International Conference on Image Processing (ICIP), Phoenix, 2016. 2221–2225
171 Xu Y, Wu Z, Chanussot J, et al. Low-rank decomposition and total variation regularization of hyperspectral video sequences. IEEE Trans Geosci Remote Sens, 2018, 56: 1680–1694
172 Yu H, Wu Z, Wei J, et al. GPU parallel implementation of gas plume detection in hyperspectral video sequences. In: Proceedings of IEEE International Geoscience and Remote Sensing Symposium (IGARSS), Valencia, 2018. 2781–2784
173 Tochon G, Chanussot J, Dalla M M, et al. Object tracking by hierarchical decomposition of hyperspectral video sequences: application to chemical gas plume tracking. IEEE Trans Geosci Remote Sens, 2017, 55: 4567–4585
174 Tan S, Liu H, Gu Y, et al. Sequential tensor decomposition for Gas tracking in Lwir hyperspectral video sequences. In: Proceedings of IEEE Workshop on Hyperspectral Imaging and Signal Processing: Evolution in Remote Sensing (WHISPERS), Amsterdam, 2019. 1–5
175 Dudley J M, Genty G, Coen S. Supercontinuum generation in photonic crystal fiber. Rev Mod Phys, 2006, 78: 1135–1184
176 Hakala T, Suomalainen J, Kaasalainen S, et al. Full waveform hyperspectral LiDAR for terrestrial laser scanning. Opt Express, 2012, 20: 7119–7127
177 Hernandez-Marin S, Wallace A M, Gibson G J. Bayesian analysis of lidar signals with multiple returns. IEEE Trans Pattern Anal Mach Intell, 2007, 29: 2170–2180
178 Suomalainen J, Hakala T, Kaartinen H, et al. Demonstration of a virtual active hyperspectral LiDAR in automated point cloud classification. ISPRS J Photogrammetry Remote Sens, 2011, 66: 637–641
179 Woodhouse I H, Nichol C, Sinclair P, et al. A multispectral canopy LiDAR demonstrator project. IEEE Geosci Remote Sens Lett, 2011, 8: 839–843
180 Wallace A M, McCarthy A, Nichol C J, et al. Design and evaluation of multispectral lidar for the recovery of arboreal parameters. IEEE Trans Geosci Remote Sens, 2013, 52: 4942–4954
181 Wei G, Shalei S, Bo Z, et al. Multi-wavelength canopy LiDAR for remote sensing of vegetation: Design and system performance. ISPRS J Photogramm Remote Sens, 2012, 69: 1–9
182 Wichmann V, Bremer M, Lindenberger J, et al. Evaluating the potential of multispectral airborne lidar for topographic mapping and land cover classification. ISPRS Ann Photogramm Remot Sens Spatial Inf Sci, 2015, 2: 113–119
183 Shi S, Song S, Gong W, et al. Improving backscatter intensity calibration for multispectral LiDAR. IEEE Geosci Remote Sens Lett, 2015, 12: 1421–1425
184 Gu Y F, Jin X D, Xiang R Z, et al. UAV-based integrated multispectral-LiDAR imaging system and data processing. Sci China Technol Sci, 2020, 63: 1293–1301
185 Pedergnana M, Marpu P R, Dalla M M, et al. Classification of remote sensing optical and LiDAR data using extended attribute profiles. IEEE J Sel Top Appl Earth Observ Remote Sens, 2012, 6: 856–865
186 Ghamisi P, Benediktsson J A, Phinn S. Land-cover classification using both hyperspectral and LiDAR data. Int J Image Data Fusion, 2015, 6: 189–215
187 Pedergnana M, Marpu P R, Dalla M M, et al. A novel technique for optimal feature selection in attribute profiles based on genetic algorithms. IEEE Trans Geosci Remote Sens, 2013, 51: 3514–3528
188 Ghamisi P, Hofle B, Zhu X X. Hyperspectral and LiDAR data fusion using extinction profiles and deep convolutional neural network. IEEE J Sel Top Appl Earth Observ Remote Sens, 2017, 10: 3011–3024
189 Rasti B, Ghamisi P, Gloaguen R. Hyperspectral and LiDAR fusion using extinction profiles and total variation component analysis. IEEE Trans Geosci Remote Sens, 2017, 55: 3997–4007
190 Rasti B, Ghamisi P, Plaza J, et al. Fusion of hyperspectral and LiDAR data using sparse and low-rank component analysis. IEEE Trans Geosci Remote Sens, 2017, 55: 6354–6365
191 Khodadadzadeh M, Li J, Prasad S, et al. Fusion of hyperspectral and LiDAR remote sensing data using multiple feature learning. IEEE J Sel Top Appl Earth Observ Remote Sens, 2015, 8: 2971–2983
192 Liao W Z, Pizurica A, Bellens R, et al. Generalized graph-based fusion of hyperspectral and LiDAR data using morphological features. IEEE Geosci Remote Sens Lett, 2015, 12: 552–556
193 Liao W, Xia J, Du P, et al. Semi-supervised graph fusion of hyperspectral and LiDAR data for classification. In: Proceedings of IEEE International Geoscience and Remote Sensing Symposium (IGARSS), Milan, 2015. 53–56
194 Liao W, Huang X, van Coillie F, et al. Processing of multiresolution thermal hyperspectral and digital color data: outcome of the 2014 IEEE GRSS data fusion contest. IEEE J Sel Top Appl Earth Observ Remote Sens, 2015, 8: 2984–2996
195 Xia J, Liao W, Du P. Hyperspectral and LiDAR classification with semisupervised graph fusion. IEEE Geosci Remote Sens Lett, 2020, 17: 666–670
196 Chen Y, Li C, Ghamisi P, et al. Deep fusion of remote sensing data for accurate classification. IEEE Geosci Remote Sens Lett, 2017, 14: 1253–1257
197 Li H, Ghamisi P, Soergel U, et al. Hyperspectral and LiDAR fusion using deep three-stream convolutional neural networks. Remote Sens, 2018, 10: 1649
198 Zhang M, Li W, Du Q, et al. Feature extraction for classification of hyperspectral and LiDAR data using patch-to-patch CNN. IEEE Trans Cybern, 2020, 50: 100–111
199 Nen M, Alpayd E N. Multiple kernel learning algorithms. J Mach Learn Res, 2011, 12: 2211–2268
200 Zhang M, Ghamisi P, Li W. Classification of hyperspectral and LIDAR data using extinction profiles with feature fusion. Remote Sens Lett, 2017, 8: 957–966
201 Zhang Y, Yang H L, Prasad S, et al. Ensemble multiple kernel active learning for classification of multisource remote sensing data. IEEE J Sel Top Appl Earth Observ Remote Sens, 2015, 8: 845–858
202 Hartzell P, Glennie C, Biber K, et al. Application of multispectral LiDAR to automated virtual outcrop geology. ISPRS J Photogrammetry Remote Sens, 2014, 88: 147–155
203 Niu Z, Xu Z G, Sun G, et al. Design of a new multispectral waveform LiDAR instrument to monitor vegetation. IEEE Geosci Remote Sens Lett, 2015, 12: 1506–1510
204 Du L, Shi S, Gong W, et al. Wavelength selection of hyperspectral LiDAR based on feature weighting for estimation of leaf

nitrogen content in rice. In: Proceedings of XXIII ISPRS Congress, Prague, 2016. 9–13
205 Du L, Shi S, Yang J, et al. Using different regression methods to estimate leaf nitrogen content in rice by fusing hyperspectral LiDAR data and laser-induced chlorophyll fluorescence data. Remote Sens, 2016, 8: 526
206 Du L, Gong W, Shi S, et al. Estimation of rice leaf nitrogen contents based on hyperspectral LIDAR. Int J Appl Earth Observation Geoinf, 2016, 44: 136–143
207 Junttila S, Kaasalainen S, Vastaranta M, et al. Investigating bi-temporal hyperspectral lidar measurements from declined trees-experiences from laboratory test. Remote Sens, 2015, 7: 13863–13877
208 Nevalainen O, Hakala T, Suomalainen J, et al. Fast and nondestructive method for leaf level chlorophyll estimation using hyperspectral LiDAR. Agr Forest Meteorol, 2014, 198: 250–258
209 Hakala T, Nevalainen O, Kaasalainen S, et al. Technical note: multispectral lidar time series of pine canopy chlorophyll content. Biogeosciences, 2015, 12: 1629–1634
210 Chen B, Shi S, Gong W, et al. Multispectral LiDAR point cloud classification: a two-step approach. Remote Sens, 2017, 9: 373
211 Puttonen E, Hakala T, Nevalainen O, et al. Artificial target detection with a hyperspectral LiDAR over 26-h measurement. Opt Eng, 2015, 54: 013105
212 Matikainen L, Karila K, Hyyppä J, et al. Object-based analysis of multispectral airborne laser scanner data for land cover classification and map updating. ISPRS J Photogrammetry Remote Sens, 2017, 128: 298–313
213 Fernandez-Diaz J, Carter W, Glennie C, et al. Capability assessment and performance metrics for the Titan multispectral mapping lidar. Remote Sens, 2016, 8: 936
214 Bakula K, Kupidura P, Jelowicki L. Testing of land cover classification from multispectral airborne laser scanning data. In: Proceedings of XXIII ISPRS Congress, Prague, 2016. 161–169
215 Wang C K, Tseng Y H, Chu H J. Airborne dual-wavelength LiDAR data for classifying land cover. Remote Sens, 2014, 6: 700–715
216 Teo T, Wu H. Analysis of land cover classification using multiwavelength LiDAR system. Appl Sci, 2017, 7: 1–20
217 Leigh H W, Magruder L A. Using dual-wavelength, full-waveform airborne lidar for surface classification and vegetation characterization. J Appl Remote Sens, 2016, 10: 045001
218 Zou X, Zhao G, Li J, et al. 3D land cover classification based on multispectral lidar point clouds. In: Proceedings of XXIII ISPRS Congress, Prague, 2016. 741–747
219 Sun J, Shi S, Chen B, et al. Combined application of 3D spectral features from multispectral LiDAR for classification. In: Proceedings of IEEE International Geoscience and Remote Sensing Symposium (IGARSS), Fort Worth, 2017. 5264–5267
220 Ekhtari N, Glennie C, Fernandez-Diaz J C. Classification of multispectral lidar point clouds. In: Proceedings of IEEE International Geoscience and Remote Sensing Symposium (IGARSS), Fort Worth, 2017. 2756–2759
221 Ekhtari N, Glennie C, Fernandez-Diaz J C, et al. Classification of airborne multispectral lidar point clouds for land cover mapping. IEEE J Sel Top Appl Earth Observ Remote Sens, 2018, 11: 2068–2078
222 Miller C I, Thomas J J, Kim J P, et al. Application of image classification techniques to multispectral lidar point cloud data. In: Proceedings of SPIE Defense + Security, Baltimore, 2016. 9832: 98320X
223 Morsy S, Shaker A, El-Rabbany A. Multispectral LiDAR data for land cover classification of urban areas. Sensors, 2017, 17: 958
224 Wang Q, Gu Y. A discriminative tensor representation model for feature extraction and classification of multispectral LiDAR data. IEEE Trans Geosci Remote Sens, 2020, 58: 1568–1586
225 Li H, Jiang T, Zhang K. Efficient and robust feature extraction by maximum margin criterion. IEEE Trans Neural Netw, 2006, 17: 157–165
226 Liu Y, Gao G, Gu Y. Tensor matched subspace detector for hyperspectral target detection. IEEE Trans Geosci Remote Sens, 2016, 55: 1967–1974
227 Veganzones M A, Cohen J E, Farias R C, et al. Nonnegative tensor CP decomposition of hyperspectral data. IEEE Trans Geosci Remote Sens, 2016, 54: 2577–2588